

The local theory of the cosmic skeleton

D. Pogosyan^{1,3}, C. Pichon^{2,3}, C. Gay²,
S. Prunet², J.F. Cardoso^{4,2}, T. Sousbie² & S. Colombi²

¹ *Department of Physics, University of Alberta, 11322-89 Avenue, Edmonton, Alberta, T6G 2G7, Canada*

² *Institut d'Astrophysique de Paris & UPMC, 98 bis boulevard Arago, 75014 Paris, France*

³ *Service d'Astrophysique, IRFU, CEA-CNRS, L'orme des merisiers, 91 470, Gif sur Yvette, France,*

⁴ *Laboratoire de Traitement et Communication de l'Information, LTCI/CNRS 46, rue Barrault, 75013 Paris, France.*

1 November 2018

ABSTRACT

The local theory of the critical lines of 2D and 3D Gaussian fields that underline the cosmic structures is presented. In the context of cosmological matter distribution the subset of critical lines of the 3D density field serves to delineate the skeleton of the observed filamentary structure at large scales. A stiff approximation used to quantitatively describe the filamentary skeleton shows that the flux of the skeleton lines is related to the average Gaussian curvature of the one D sections of the field, much in the same way as the density of the peaks. The distribution of the length of the critical lines with threshold is analyzed in detail, while the extended descriptors of the skeleton - its curvature and its singular points, are introduced and briefly described. Theoretical predictions are compared to measurements of the skeleton in realizations of Gaussian random fields in 2D and 3D. It is found that the stiff approximation predicts accurately the shape of the differential length, allows for analytical insight, and explicit closed form solutions. Finally, it provides a simple classification of the singular points of the critical lines: i) critical points; ii) bifurcation points; iii) slopping plateaux.

1 INTRODUCTION

The concept of random fields is central to cosmology. Random fields both provide initial conditions for the evolution of the matter distribution in the Universe, and represent how the observed signals manifest themselves in 3D, (e.g., in the galaxy or matter density inhomogeneities that form the Large Scale Structure (LSS)), or on the 2D sky (e.g. for the Cosmic Microwave Background (CMB) temperature and polarization, the convergence or shear in weak lensing maps). In the modern cosmological theories where initial seeds for inhomogeneities observed as cosmic structures have quantum origin, the fields of initial density fluctuations (and velocities) are Gaussian. Subsequent evolution retains Gaussianity for the observables that evolve linearly (CMB, very Large Scale Structure) while developing non-Gaussian signature if non-linear effects are involved (e.g. lensing and LSS at smaller scales).

While comparing the observational data to cosmological theory, in particular in order to estimate parameters of cosmological models, the emphasis is traditionally placed on the statistical descriptors of the random fields. For Gaussian fields the two-point correlation function or the power spectrum provide full statistical information, while non-Gaussian properties may be reflected in multi-point correlations. The understanding and the description of the morphology of structures in our Universe, on the other hand, calls for the studies of the *geometry* and *topology* of random fields. This subject has an extensive history from the early description of the one-dimensional radio signal time-streams in 1940's, to the study of the 2D ocean wave patterns in 1960's (Longuet-Higgins 1957) to 3D dimensional fields (Adler 1981) that found the most fruitful application in cosmology (Arnol'd et al. 1981; Bardeen et al. 1986). The most prominent geometrical objects in a typical realization of a random field are rare events - regions of unusually high or low values of the field. The rare events are usually related to the most spectacular observed objects - clusters of galaxies at low z , large protogalaxies at high- z or extensive voids. They are associated with the neighbourhoods of extrema - maxima or minima - making studies of such *critical* points the first step in understanding typical geometry of a field (Kaiser 1984; Bardeen et al. 1986; Regos & Szalay 1995; Scannapieco et al. 2006). The behaviour of the field in the neighbourhood of a rare peak is highly correlated with the peak properties, which allows to describe not only extrema but the extended peak-patch region (Bond & Myers 1996a) as a point process that involves the field and its successive derivatives. Including the shear flow into consideration gives a compelling application of the geometry of rare events to the description of cluster formation through the peak-patch collapse (Bond & Myers 1996b).

The rare events reflect the organization of the field around them and by and large determine the way the high (low) field regions are interconnected by the bridges of enhanced field values. In application to cosmology, the ‘‘Cosmic Web’’ picture emerges, which relates the observed clusters of galaxies, and filaments that link them, to the geometrical properties of the initial density field that are enhanced but not yet destroyed by the still mildly non-linear evolution on supercluster scales (Bond et al. 1996). The study of the connectivity of filamentary structures reveal the role of the remaining type of critical points, the saddle extrema, in establishing, in particular, the percolation properties of the Web (Colombi et al. 2000). The next step naturally involves describing the statistical properties of these filamentary structures (Pogosyan et al. 1998; Schmalzing et al. 1999) and developing techniques for mapping the filaments in the simulation and data. Novikov et al. (2006) presented a 2D algorithm to trace the filaments of a density field while introducing the *skeleton* as the set of locally defined critical lines emanating from the critical points. Sousbie et al. (2008) (hereafter SPCNP) extended the local theory and algorithm to three dimensions and provided the foundation for this work while introducing the ‘‘stiff’’ approximation. Recently, Sousbie et al. (2008) presented an algorithm to map out a fully connected version of the skeleton that is defined according to the global properties as the lines of intersections of the patches (see also Aragón-Calvo et al. (2007), Platen et al. (2007) for alternative algorithms). This approach connects the study of the filamentary structure to the geometrical and topological aspects of the theory of gradient flows (Jost 2008) and returns the focus to the notions of peak and void patches.

This paper presents a consistent local theory for the cosmic skeleton, while focusing on the stiff approximation to compute the differential length of the skeleton as a function of the contrast and modulus of the gradient of the field. It allows us to define precisely how the properties of the skeleton depend analytically on the underlying spectral parameters, and understand what type of line prevails where. The crucial advantage of the local approach to the critical lines is that it allows to cast the statistical treatment of the linear objects as a point process that involves the field and its derivatives, which allows for analytical insight, and explicit closed form solutions. Our purpose is to construct the theory of critical lines of a given field corresponding to an intermediate representation of the field, which is more extended than the knowledge of the critical points.

The organization of the paper is the following. Section 2 classifies the various critical lines in 2D and 3D, connects the average length in a unit volume to the flux of the skeleton lines and, within the stiff approximation, to the average Gaussian curvature of the field in transverse sections. It also discusses the meaning of this approximation. Section 3 calculates the differential length of all sets of critical lines in 2D, while Section 4 investigates the corresponding 3D set of critical lines. More generally, the expression for the differential length of the N dimensional skeleton is sketched in Appendix A. Section 5 introduces the extended descriptors of the skeleton, Section 5.3 describes their singular points, while Section 6 provides the discussion and the summary. Appendix D gives the general method for obtaining in close form the joint distribution of the field and any combination of its derivative tensors in arbitrary dimensions. In particular, it exhibits all the statistical invariants and their dependence on the spectral parameters.

2 THE CRITICAL LINES AND THE SKELETON OF A 3D RANDOM FIELD

2.1 Local definition and classification

The subject of our investigation is a random field, $\rho(\mathbf{r})$, that in a cosmological setting describes, for example, the density of the matter in the Universe, or the projected distribution of Cosmic Microwave light on the celestial sphere. Our focus is on the geometrical properties of the critical lines, that connect extrema of the field mapping out the filamentary ridges and valleys of the field. SPCNP have introduced the definition of the *local critical lines* as the set of points where the gradient of the density, $\nabla\rho$, is an eigenvector of its Hessian matrix, \mathcal{H} , $\mathcal{H} \cdot \nabla\rho = \lambda\nabla\rho$ i.e, the gradient and one of the principal curvature axes are collinear. Formally, this can be specified by a set of equations

$$\mathbf{S} \equiv (\nabla\rho \cdot \mathcal{H}) \cdot \boldsymbol{\epsilon} \cdot (\nabla\rho) = \mathbf{0} , \quad (1)$$

where $\boldsymbol{\epsilon}$ is the fully antisymmetric (Levi-Civita) tensor of rank N . In general \mathbf{S} is an antisymmetric $N - 2$ tensor.

In 3D, the function \mathbf{S} is vector-valued, $S^i = \sum_{klm} \epsilon^{ikl} (\nabla_m \rho) \mathcal{H}^m_k (\nabla_l \rho)$. However, zeroes of \mathbf{S} determine a set of lines rather than isolated points. Let us consider the behaviour of \mathbf{S} function in the neighbourhood of a point $\mathbf{r} = \mathbf{0}$ that satisfies criticality condition $\mathbf{S}(\mathbf{0}) = \mathbf{0}$:

$$\mathbf{S}(\delta\mathbf{r}) \approx \mathbf{0} + \sum_k (\nabla_k \mathbf{S}) \delta r^k . \quad (2)$$

In our case, under the condition $S^i = 0$, the matrix $\nabla_k S^i$ by definition possesses the *left* null-vector, furnished by the density gradient, $\sum_i \nabla_i \rho (\nabla_k S^i) = 0$; hence the gradients ∇S^i are not linearly independent. Consequently, there is a non-trivial solution for the *right* null-vector $\sum_k (\nabla_k S^i) \delta r^k = \mathbf{0}$, which determines the local direction of the line along which the criticality condition is maintained, $\mathbf{S}(\delta\mathbf{r}) = \mathbf{0}$. The critical lines intersect where $\nabla_k S^i$ admits more than one independent *right* null-vector.

When we take the eigenvalues of the Hessian to be sorted, $\lambda_1 \geq \lambda_2 \geq \lambda_3$, the gradient of the field at the critical line may be found aligned with the first, second, or third eigenvector. This gives rise to the classification of the critical lines based on the choice of the eigenvector aligned with the gradient, that becomes more fine grained when the magnitudes of the eigenvalues are taken into account. Namely, we distinguish *primary* critical lines, which correspond to $\nabla\rho$ being aligned with the direction in which the field is the least curved, i.e where the eigenvalue is the smallest in magnitude, and *secondary* critical lines at which $\nabla\rho$ is aligned with the eigenvalues of larger magnitude. The primary type consists of

Type	Alignment	Condition
Primary	Skeleton:	$\mathcal{H} \cdot \nabla \rho = \lambda_1 \nabla \rho$ $\lambda_1 + \lambda_2 \leq 0$
	Inter-skeleton:	$\mathcal{H} \cdot \nabla \rho = \lambda_2 \nabla \rho$ $\lambda_1 + \lambda_2 > 0$ and $\lambda_3 + \lambda_2 < 0$
	Anti-skeleton:	$\mathcal{H} \cdot \nabla \rho = \lambda_3 \nabla \rho$ $\lambda_3 + \lambda_2 \geq 0$
Secondary		$\mathcal{H} \cdot \nabla \rho = \lambda_2 \nabla \rho$ $\lambda_1 + \lambda_2 \leq 0$
		$\mathcal{H} \cdot \nabla \rho = \lambda_3 \nabla \rho$ $\lambda_1 + \lambda_2 \leq 0$
		$\mathcal{H} \cdot \nabla \rho = \lambda_1 \nabla \rho$ $\lambda_1 + \lambda_2 > 0$ and $\lambda_3 + \lambda_2 < 0$
		$\mathcal{H} \cdot \nabla \rho = \lambda_3 \nabla \rho$ $\lambda_1 + \lambda_2 > 0$ and $\lambda_3 + \lambda_2 < 0$
		$\mathcal{H} \cdot \nabla \rho = \lambda_1 \nabla \rho$ $\lambda_3 + \lambda_2 \geq 0$
		$\mathcal{H} \cdot \nabla \rho = \lambda_2 \nabla \rho$ $\lambda_3 + \lambda_2 \geq 0$

Table 1. the classification of the critical lines in 3D.

(i) The *skeleton*, that has the gradient in the λ_1 direction and is limited to the region $|\lambda_1| \leq |\lambda_2|$, which translates to the condition $\lambda_1 + \lambda_2 \leq 0$. The skeleton has always eigenvalues in the directions transverse to $\nabla \rho$ negative, $\lambda_3 \leq \lambda_2 \leq 0$ and corresponds to the filamentary ridges spreading from the maxima in the direction of the slowest descent.

(ii) The *anti-skeleton*, that has the gradient in the λ_3 direction and is restricted to the region $|\lambda_3| \leq |\lambda_2|$, i.e. $\lambda_3 + \lambda_2 \geq 0$. In the directions transverse to $\nabla \rho$ the anti-skeleton has always positive curvature $\lambda_1 \geq \lambda_2 \geq 0$. It corresponds to the filamentary valleys spreading from the minima in the direction of the slowest ascent. Anti-skeleton can be viewed as a skeleton of the $-\rho$ field.

(iii) The *intermediate skeleton* along which the gradient is aligned with the middle eigen-direction of the Hessian where this direction is the shallowest $|\lambda_2| < |\lambda_1|, |\lambda_3|$, i.e. $-\lambda_1 < \lambda_2 < -\lambda_3$. This conditions is only possible in saddle-like regions where $\lambda_1 > 0$ and $\lambda_3 < 0$.

The formal classification of the critical lines is summarized in Table 1.

2.2 The average flux (length per unit volume) of the critical lines

As the average number density is the fundamental quantity that describes point events, e.g. extrema of a field, conversely the most important characterization of the critical lines or skeleton is their flux, *i.e.* the number of critical lines intersecting a given oriented surface¹. This flux is equivalent to the length of the lines per unit volume. Following NCD and SPCNP we shall preferentially use the latter terminology as it highlights that we deal with the first geometrical parameter, the length, of the lines. The subsequent parameters of these linear objects are the curvature, and, in 3D, the torsion.

In this paper we consider ρ to be a homogeneous and isotropic Gaussian random field of zero mean, described by the power spectrum $P(k)$. In the statistical description of the skeleton of the field ρ , several linear scales are involved

$$R_0 = \frac{\sigma_0}{\sigma_1}, \quad R_* = \frac{\sigma_1}{\sigma_2}, \quad \tilde{R} = \frac{\sigma_2}{\sigma_3}, \quad \hat{R} = \frac{\sigma_3}{\sigma_4}, \quad (3)$$

$$\text{where } \sigma_0^2 = \langle \rho^2 \rangle, \quad \sigma_1^2 = \langle (\nabla \rho)^2 \rangle, \quad \sigma_2^2 = \langle (\Delta \rho)^2 \rangle, \quad \sigma_3^2 = \langle (\nabla \Delta \rho)^2 \rangle, \quad \text{and generally } \sigma_p^2 = \frac{2\pi^{D/2}}{\Gamma[D/2]} \int_0^\infty k^{2p} P(k) k^{D-1} dk. \quad (4)$$

These scales are ordered $R_0 \geq R_* \geq \tilde{R} \geq \dots$. The first two have well-known meanings of typical separation between zero-crossing of the field R_0 and mean distance between extrema, R_* (Bardeen & al. 1986), and the third one, \tilde{R} is, by analogy, the typical distance between the inflection points. These three are the only ones that are involved in determination of the length of the critical lines. The higher order scale \hat{R} appear only in computation of the curvature and the torsion (see Section 5).

Let us define a set of spectral parameters that depend on the shape of the underlying power spectrum. Out of these five scales four dimensionless ratios may be constructed that are intrinsic parameters of the theory

$$\gamma \equiv \frac{R_*}{R_0} = \frac{\sigma_1^2}{\sigma_0 \sigma_2}, \quad \tilde{\gamma} \equiv \frac{\tilde{R}}{R_*} = \frac{\sigma_2^2}{\sigma_3 \sigma_1}, \quad \hat{\gamma} \equiv \frac{\hat{R}}{\tilde{R}} = \frac{\sigma_3^2}{\sigma_4 \sigma_2}, \quad \text{and generally } \gamma_{p,q} = \frac{\sigma_{p+q}^2}{\sigma_p \sigma_q}. \quad (5)$$

From the geometrical point of view γ specifies how frequently one encounters a maximum between two zero crossings of the field, while $\tilde{\gamma}$ describes, on average, how many inflection points are between two extrema. From a statistical perspective, γ 's are the cross-correlation coefficients between the field and its derivatives at the same point (see Appendix D).

$$\gamma = \frac{\langle \rho \Delta \rho \rangle}{\sigma_0 \sigma_2}, \quad \tilde{\gamma} = \frac{\langle \nabla \rho \cdot \nabla \Delta \rho \rangle}{\sigma_1 \sigma_3}, \quad \dots \quad (6)$$

¹ For M dimensional objects in N dimensional space, in general, one counts the average number of intersections between objects M and N-M dimensional surfaces, per unit N-M volume. From a statistical point of view this constitutes a *point* process that can be evaluated knowing the distribution of the field and some of its derivatives at one arbitrary point only.

For Gaussian fields, these parameters can be easily calculated from the power spectrum. All γ 's range from zero to one. For reference, for the power-law spectra with index $n > -3$, smoothed at small scales with a Gaussian window, $\gamma = \sqrt{(n+3)/(n+5)}$, $\tilde{\gamma} = \sqrt{(n+5)/(n+7)}$. Note that cosmologically relevant density power spectra have $n > -3$ and, thus, while γ can attain low values, $\tilde{\gamma}$ are always close to unity².

Let us introduce the dimensionless quantities for the field and its derivatives as well as for the functions S^i and their gradients ∇S^i :

$$\sigma_0 x \equiv \rho, \quad \sigma_1 x_k \equiv \nabla_k \rho, \quad \sigma_2 x_{kl} \equiv \nabla_k \nabla_l \rho, \quad \sigma_3 x_{klm} \equiv \nabla_m \nabla_l \nabla_k \rho, \quad \sigma_2 \sigma_1^2 s^i \equiv S^i, \quad \sigma_2^2 \sigma_1 \nabla s^i \equiv \nabla S^i, \quad \sigma_4 \sigma_1^2 \nabla \nabla s^i \equiv \nabla \nabla S^i, \quad (7)$$

giving

$$s^i = \sum_{klm} \epsilon^{imk} x_{ml} x_l x_k, \quad \text{and} \quad \nabla_m s^i = \sum_{klm} \epsilon^{imk} (\tilde{\gamma}^{-1} x_{nlm} x_l x_k + [x_{nl} x_{lm} x_k + x_{nl} x_{km} x_l]). \quad (8)$$

Note the specific choice of scaling for ∇S which is convenient in view of the subsequent development of the so-called ‘‘stiff’’ approximation. SPCNP has shown that in terms of these dimensionless quantities, the *cumulative* length per unit volume of the total set of critical lines below the threshold η is given by

$$\mathcal{L}(\eta) = \left(\frac{1}{R_*}\right)^2 \int_{-\infty}^{\eta} dx \int d^3 x_k d^6 x_{kl} d^{10} x_{klm} |\nabla s^i \times \nabla s^j| P(x, x_k, x_{kl}, x_{klm}) \delta_D(s^i(x_k, x_{kl}, x_{klm})) \delta_D(s^j(x_k, x_{kl}, x_{klm})), \quad (9)$$

where a pair $\nabla s^i, \nabla s^j$ can be chosen arbitrarily as long as it is linearly independent. In this equation $|\nabla s^i \times \nabla s^j|$ reflects the inverse characteristic area orthogonal to a critical line per one such line while the two δ_D -functions account for the critical line condition (1). For the complete set of critical lines, there are no restriction to the region of integration. If one is interested in a particular type of the critical lines, the integration should be restricted to the regions consistent with Table 1. The *differential* length (per unit volume) is simply given by the derivative of equation (9) with respect to η :

$$\frac{\partial \mathcal{L}}{\partial \eta} = \left(\frac{1}{R_*}\right)^2 \int d^3 x_k d^6 x_{kl} d^{10} x_{klm} |\nabla s^i \times \nabla s^j| P(\eta, x_k, x_{kl}, x_{klm}) \delta_D(s^i(x_k, x_{kl}, x_{klm})) \delta_D(s^j(x_k, x_{kl}, x_{klm})), \quad (10)$$

while the total length of critical lines is

$$L \equiv \mathcal{L}(\infty) = \int_{-\infty}^{\infty} d\eta \frac{\partial \mathcal{L}}{\partial \eta}. \quad (11)$$

Since for Gaussian field, the derivatives of even order are uncorrelated with the odd orders, the joint distribution function $P(x, x_k, x_{kl}, x_{klm})$ entering equation (9) is factorized as

$$P(x, x_k, x_{kl}, x_{klm}) = P_0(x, x_{kl}) P_1(x_k, x_{klm}). \quad (12)$$

In P_0 , the only dependence on the power spectrum of the field is through the parameter γ (c.f. equation (5)) that describes the correlation between the field and its second derivatives. Similarly $P_1(x_k, x_{klm})$ only involves $\tilde{\gamma}$ which describes the correlation between the gradient of the field and its third derivatives. Therefore, $\partial \mathcal{L} / \partial \eta$ depends only on η , \tilde{R} , γ and $\tilde{\gamma}$. The integrated length, L may depend only on $\tilde{\gamma}$ and \tilde{R} since the marginalization of $P_0(\eta, x_{kl})$ over η eliminates the dependency over γ .

2.3 The ‘‘stiff’’ filament approximation

Let us look at the dependence of the length of the critical lines on characteristic scales of the field in more detail. The R_*^{-2} factor that appeared in equation (10) reflect our choice of dimensionless variables (8) and is suggestive but not yet conclusive since $|\nabla s^i \times \nabla s^j|$ that includes third derivative terms, depends also on the other scale, \tilde{R} . Let us write formally

$$\nabla s^i \times \nabla s^j = \tilde{\gamma}^{-2} \mathbf{A}(x_k, x_{kl}, x_{klm}) + \tilde{\gamma}^{-1} \mathbf{B}(x_k, x_{kl}, x_{klm}) + \mathbf{C}(x_k, x_{kl}). \quad (13)$$

If the third derivatives are important and the first term dominates, then the length scaling $L \propto \tilde{\gamma}^{-2} R_*^{-2} = \tilde{R}^{-2}$ would reflect the mean separation between the inflection points, \tilde{R} . Indeed, by definition the local skeleton is almost straight within a volume that has one inflection point $\sim \tilde{R}^3$. A straight segment through such volume has length $\sim \tilde{R}$, thus the expected length per unit volume is $\sim 1/\tilde{R}^2$. But if the last term dominates statistically, the length per unit volume of the skeleton will scale as $L \propto R_*^{-2}$ that can be interpreted that the critical lines are almost straight within a large volume volume $\sim R_*^3$ containing one extremum. This is consistent with observation that the integral term does not depend on the third derivatives, thus inflection points play no role, and any dependence on $\tilde{\gamma}$ drops out.

Which regime holds can be established by measuring the dependence of the critical lines length in the simulations as a function of smoothing length for different spectral indexes. For the power-law spectra with Gaussian smoothing at the radial scale σ , in 3D, $R_* = \sqrt{2}\sigma/\sqrt{n+5}$, while $\tilde{R} = \sqrt{2}\sigma/\sqrt{n+7}$. The measurements in SPCNP found that $L \propto (n+5.5)\sigma^{-2}$ over the range of spectral indexes relevant to cosmology, which points at the subdominant nature played by the third derivatives. In the ‘‘stiff’’ approximation we omit the third derivative, effectively assuming that the Hessian can be treated as constant

² Cosmological density fields, therefore, have of order one inflection point per extremum, unlike, for, example, a mountain range, where one encounters many inflection points on a way from a mountain top to the bottom; see also Section 4.4.

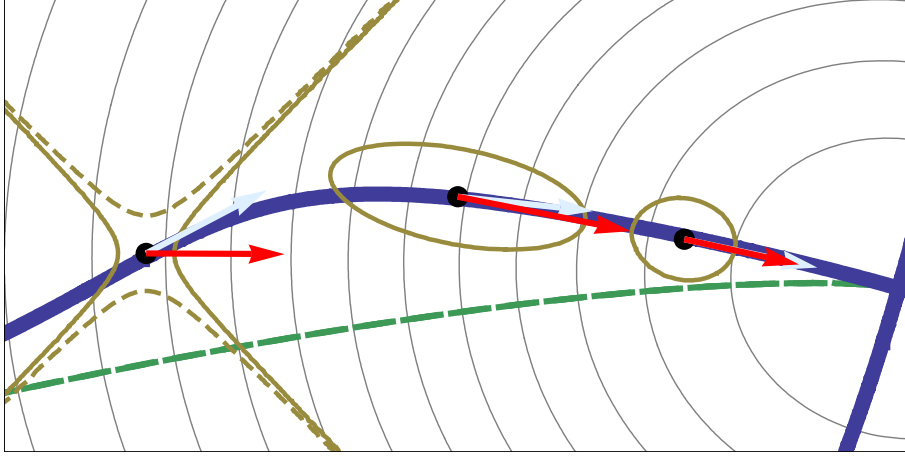


Figure 1. The neighbourhood of a local critical line (thick blue line). This is a zoomed section of the wide patch shown in Figure 2. Thin lines are isocontours of the field. Three sample points are investigated in detail. The signature, orientation and the magnitude of the local Hessian are represented by the golden shapes. Near the maximum on the right edge, the signature of the eigenvalues of the Hessian is $(-1,-1)$, which is shown by ellipses oriented according to eigen-directions with longer semi-axis along the direction of the least curvature. At the leftmost point the eigenvalue signature is “saddle-like”, $(1,-1)$, which is represented by a pair of hyperbolae, also oriented with respect to eigen-directions. By definition, on the critical line the gradient of the field $\nabla\rho$, shown by red arrows, is aligned with one of the eigen-directions (i.e the axis of the ellipse or hyperbola in the graph). The light cyan arrows are the tangent vectors to the critical line $\propto \epsilon \cdot \nabla S$, while stiff approximation to them would be parallel to the gradient. The direction of the critical line is close to the gradient when it follows the ridge near the maximum, but slides at an angle in the “saddle-like” region, before joining the saddle extremal point beyond the left edge of the plot (see Figure 2). Note that the gradient line that takes us to the same saddle as a segment of the global skeleton (dashed green) does not follow the ridge too closely in this instance.

during the evaluation of ∇s . This picture corresponds to a skeleton connecting extrema with relatively straight segments. In the “stiff” approximation, equation (10) becomes

$$\frac{\partial \mathcal{L}}{\partial \eta} \approx \left(\frac{1}{R_*} \right)^2 \int d^3 x_k d^6 x_{kl} |C(x_k, x_{kl})| P_0(\eta, x_{kl}) P_1(x_k) \delta_D \left(s^i(x_k, x_{kl}) \right) \delta_D \left(s^j(x_k, x_{kl}) \right). \quad (14)$$

The differential length is then only the function of γ times L .

The “stiff” approximation can be looked at from another perspective. By definition at a point on a local critical line, two of the characteristic directions defined for the field, namely, the direction of the gradient, $\nabla\rho$, and one chosen eigen direction of the Hessian, \mathcal{H} , must coincide. But the direction of the critical line itself, given by $\nabla S^i \times \nabla S^j$, is not, in general, aligned with the gradient of the field. Local critical lines are not the gradient lines, and in this sense they differ from the skeleton lines defined globally as void-patch intersections (Sousbie et al. 2008). In the “stiff” approximation, however, $(\nabla_m s^i)_{\text{stiff}} \approx \sum_{kln} \epsilon^{ink} [x_{nl} x_{lm} x_k + x_{nl} x_{km} x_l]$ and $[(\nabla s^i)_{\text{stiff}} \times (\nabla s^j)_{\text{stiff}}] \times \nabla\rho = 0$, *i.e.* it is parallel to the gradient. Figure 1 shows the details of the calculations for the high-resolution segment of the 2D field. Thus, the essence of the stiff approximation lies in the assumption that the mismatch between the critical lines and gradient directions is statistically small. As Figure 2, which contains an extended view of the same field, illustrates, this assumption holds particularly well for the primary critical lines which more closely correspond to the intuitive picture of sharp ridges and deep valleys. Indeed, at a primary line the gradient points to the least curved direction, *i.e.* in some sense in the direction in which the changes of the field properties are the slowest. Therefore one can expect that this is the direction in which the condition of criticality will be maintained, *i.e.* which the critical line itself will follow. Figure 2 shows that the primary lines start to deviate from the gradient flow mostly towards their end points when the curvature of the field along the line becomes comparable in magnitude to the transverse one. Secondary critical lines are much less certain to follow the gradient, sometimes exhibiting a “sliding” behaviour, on occasion almost orthogonal to the gradient, as a loop-like secondary line near the right saddle in Figure 2 exhibits. So the stiff approximation for the secondary lines should be taken with more caution, although we include them for completeness.

The stiff approximation provides a framework to compute the total differential length of the critical lines and the local skeleton almost completely analytically. In the next two sections we will carry this calculation in two and three dimensions and argue that it can straightforwardly be extended in N dimensions (see Appendix A). In what follows we shall omit in the derivation for brevity the $1/R_*$ (in 2D) and $1/R_*^2$ (in 3D) factors, but keep in mind that all the length quantities below scale accordingly. In section 4.4, after the computational machinery is developed, we return to the role the third derivative may play in description of the critical lines.

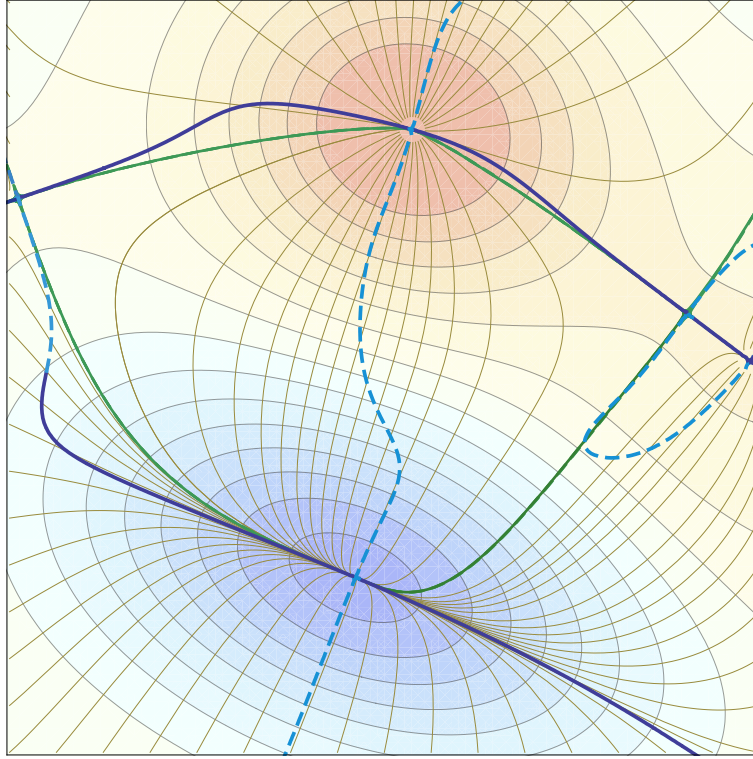


Figure 2. An example of a generic patch of a 2D field. The underlying isocontours correspond to the density field. The thin gold lines are the gradients lines of the field. The blue lines is the local set of critical lines, given by the solution of $\mathcal{S} \equiv (\mathcal{H} \cdot \nabla \rho) \times \nabla \rho = \mathbf{0}$. Primary lines are shown in solid and the secondary lines are dashed. The green lines correspond to global critical lines: the skeleton and the anti skeleton, which delineate a special bundle of gradient lines (Jost 2008) at the intersection of a peak patch and a void patch. The primary local lines follow fairly well the gradient lines, noticeably near the extrema, where the “stiff” approximation holds best. In contrast, the approximation worsens for the secondary critical lines. The main distinction between the global and local skeletons is that the global one follows the everywhere smooth gradient line that uniquely connects a maximum to a saddle, at the cost of deviating from being exactly on the ridge (see how in the vicinity of the minimum at the bottom, the right green line does not follow the trough) The local skeleton tries to delineate the ridges as far from extrema as possible, but then the lines that follow this local procedure from different extrema do not meet and have to rather suddenly reconnect. A particularly striking example of this is the loop on the right hand side. A zoomed view of the area left to the top maximum is shown in Figure 1.

Type		Alignment	Condition
Primary	Skeleton:	$\mathcal{H} \cdot \nabla \rho = \lambda_1 \nabla \rho$	$\lambda_1 + \lambda_2 \leq 0$
	Anti-skeleton:	$\mathcal{H} \cdot \nabla \rho = \lambda_2 \nabla \rho$	$\lambda_1 + \lambda_2 > 0$
Secondary		$\mathcal{H} \cdot \nabla \rho = \lambda_2 \nabla \rho$	$\lambda_1 + \lambda_2 \leq 0$
		$\mathcal{H} \cdot \nabla \rho = \lambda_1 \nabla \rho$	$\lambda_1 + \lambda_2 > 0$

Table 2. the classification of the critical lines in 2D.

3 CRITICAL LINES OF 2D FIELDS

Even though the large scale structures of the universe are three dimensional, other important observed data sets involve 2D maps such as the cosmic microwave background or lensing convergence maps. Hence analyzing the local statistical properties of filaments in two dimensions is astrophysically well motivated. The 2D case is also a convenient starting point to introduce the details of the calculations that can be generalized to 3D and higher dimensions.

The 2D case affords several simplifications over the 3D case. In 2D, S is a (pseudo) scalar function and its zero level, orthogonal to ∇S , determines the critical lines. The expression for the differential length simplifies to

$$\frac{\partial \mathcal{L}}{\partial \eta} = \frac{1}{R_*} \int d^2 x_k d^3 x_{kl} d^4 x_{klm} |\nabla s| P(\eta, x_k, x_{kl}, x_{klm}) \delta_D(s(x_k, x_{kl})) . \quad (15)$$

There are just four types of critical lines: two primary, the skeleton and the anti-skeleton, and two corresponding secondary ones. The classification of the 2D critical lines is summarized in Table 2. We shall focus on the most interesting primary lines in the main text, leaving the secondaries to the Appendix B. In Figure 2 the critical lines of different types are shown for an example generic patch of a 2D field.

3.1 The differential length of the critical lines of 2D fields

For 2D Gaussian fields, the calculation of the length of the critical lines can be carried almost completely analytically in the stiff approximation.

3.1.1 Direct derivation in the field's frame

Let us first proceed in the original coordinate frame. Defining

$$s = x_1 x_2 (x_{11} - x_{22}) + x_{12} (x_2^2 - x_1^2) = 2w x_1 x_2 + x_{12} (x_2^2 - x_1^2), \quad (16)$$

the stiff approximation to ∇s involves only up to second derivatives of the field

$$|\nabla s|^2 = (x_1^2 + x_2^2) (w^2 + x_{12}^2) \left(u^2 + 4(w^2 + x_{12}^2) - 4 \frac{2x_1 x_2 x_{12} + w(x_1^2 - x_2^2)u}{x_1^2 + x_2^2} u \right), \quad (17)$$

and equation (15) becomes explicitly

$$\frac{\partial \mathcal{L}}{\partial \eta} = \frac{16}{(2\pi)^3 \sqrt{1-\gamma^2}} \exp\left[-\frac{\eta^2}{2}\right] \iiint \iiint dudw dx_{12} dx_1 dx_2 |\nabla s| \delta_D(s) \exp\left[-\frac{(u-\gamma\eta)^2}{2(1-\gamma^2)} - 4w^2 - 4x_{12}^2 - x_1^2 - x_2^2\right], \quad (18)$$

where the second derivatives are described using $u = -(x_{11} + x_{22})$, $w = (x_{11} - x_{22})/2$ and x_{12} . Let us integrate over x_{12} using the δ_D -function, which leads to a substitution $x_{12} \rightarrow (2x_1 x_2 w)/(x_1^2 - x_2^2)$ with the Jacobian $|1/(x_1^2 - x_2^2)|$. Then equation (18) becomes

$$\frac{\partial \mathcal{L}}{\partial \eta} = \frac{16}{(2\pi)^3 \sqrt{1-\gamma^2}} \exp\left[-\frac{\eta^2}{2}\right] \iiint \iiint dudw dx_1 dx_2 \frac{|\nabla s|}{|x_1^2 - x_2^2|} \exp\left[-\frac{(u-\gamma\eta)^2}{2(1-\gamma^2)} - 4w^2 \frac{(x_1^2 + x_2^2)^2}{(x_1^2 - x_2^2)^2} - x_1^2 - x_2^2\right], \quad (19)$$

where

$$|\nabla s|^2 = w^2 \frac{(x_1^2 + x_2^2)^3}{(x_1^2 - x_2^2)^2} \left(u + 2w \frac{(x_1^2 + x_2^2)}{(x_1^2 - x_2^2)} \right)^2. \quad (20)$$

Let us now substitute³

$$\tilde{w} = w \frac{(x_1^2 + x_2^2)}{(x_1^2 - x_2^2)}, \quad \text{noting that } \tilde{w}^2 = (w^2 + x_{12}^2), \quad (21)$$

to obtain

$$\frac{\partial \mathcal{L}}{\partial \eta} = \frac{16}{(2\pi)^3 \sqrt{1-\gamma^2}} \exp\left[-\frac{\eta^2}{2}\right] \iiint \iiint dud\tilde{w} dx_1 dx_2 \frac{|\tilde{w}(u+2\tilde{w})|}{\sqrt{x_1^2 + x_2^2}} \exp\left[-\frac{(u-\gamma\eta)^2}{2(1-\gamma^2)} - 4\tilde{w}^2 - x_1^2 - x_2^2\right]. \quad (22)$$

The integration over the first derivatives is now easily performed in the polar coordinates of the x_1, x_2 plane to give

$$\frac{\partial \mathcal{L}}{\partial \eta} = \frac{2}{\pi^{3/2} \sqrt{1-\gamma^2}} \exp\left[-\frac{\eta^2}{2}\right] \int_{-\infty}^{\infty} \int_{-\infty}^{\infty} dud\tilde{w} |\tilde{w}(u+2\tilde{w})| \exp\left[-\frac{(u-\gamma\eta)^2}{2(1-\gamma^2)} - 4\tilde{w}^2\right]. \quad (23)$$

This is the final integral form which can be easily investigated in the u, \tilde{w} plane.

3.1.2 Derivation in the Hessian eigenframe

To generalize the derivation to higher dimensions we note that one can just perform all the calculations in the Hessian eigenframe. We shall denote all quantities *evaluated* in the eigenframe with tilde, e.g., $\tilde{x}_{11} (= \lambda_1)$, $\tilde{x}_{22} (= \lambda_2)$, \tilde{u} , \tilde{w} , \tilde{x}_1 , \tilde{x}_2 . What must be taken into account is that, in general, these quantities are not Gaussian random variables (while the corresponding ones in the fixed frame are), since the transformation from the fixed to eigenframe is non-linear. The Gaussian nature is only preserved for \tilde{u} , \tilde{x}_1 , \tilde{x}_2 . In the Hessian eigenframe $\tilde{x}_{12} = 0$. From equations (16-17)

$$\tilde{s} = \tilde{x}_1 \tilde{x}_2 (\tilde{x}_{11} - \tilde{x}_{22}) = \tilde{x}_1 \tilde{x}_2 (\lambda_1 - \lambda_2) = 2\tilde{x}_1 \tilde{x}_2 \tilde{w}, \quad \left| \tilde{\nabla} s \right| = |\tilde{w}| \sqrt{(\tilde{u} + 2\tilde{w})^2 \tilde{x}_1^2 + (\tilde{u} - 2\tilde{w})^2 \tilde{x}_2^2}. \quad (24)$$

In equation (15) the averaging is now carried over the distribution of the eigenvalues with the measure $\pi(\lambda_1 - \lambda_2)$ (Doroshkevich 1970) that accounts for eigenvalues being sorted, $\lambda_1 \geq \lambda_2$:

$$\frac{\partial \mathcal{L}}{\partial \eta} = \frac{8 \cdot 2 \cdot \pi}{(2\pi)^3 \sqrt{1-\gamma^2}} \exp\left[-\eta^2/2\right] \iiint \iiint (\lambda_1 - \lambda_2) d\lambda_1 d\lambda_2 d\tilde{x}_1 d\tilde{x}_2 \left| \tilde{\nabla} s \right| \delta_D(\tilde{s}) \exp\left[-\frac{(\tilde{u} - \gamma\eta)^2}{2(1-\gamma^2)} - 4\tilde{w}^2 - \tilde{x}_1^2 - \tilde{x}_2^2\right], \quad (25)$$

³ here we made a choice of sign. Now in the coordinate frame that has the first direction aligned with the gradient of the field, i.e. $x_2 = 0$, $\tilde{w} = (x_{11} - x_{22})/2$, while in the frame that has gradient aligned with the second direction, $x_1 = 0$, $\tilde{w} = (x_{22} - x_{11})/2$

or in terms of \tilde{u}, \tilde{w}

$$\frac{\partial \mathcal{L}}{\partial \eta} = \frac{16}{(2\pi)^2 \sqrt{1-\gamma^2}} \exp[-\eta^2/2] \iiint |\tilde{w}| d\tilde{u} d\tilde{w} d\tilde{x}_1 d\tilde{x}_2 \left| \nabla \tilde{s} \right| \delta_D(\tilde{s}) \exp \left[-\frac{(\tilde{u} - \gamma\eta)^2}{2(1-\gamma^2)} - 4\tilde{w}^2 - \tilde{x}_1^2 - \tilde{x}_2^2 \right]. \quad (26)$$

In the argument of the delta-function in equation (26) \tilde{w} can be zero only at special field points, not at a generic point on a skeleton. So vanishing \tilde{s} requires either $\tilde{x}_1 = 0$ or $\tilde{x}_2 = 0$ which describes, as expected, that in the Hessian eigenframe one of the component of the gradient vanishes on the critical line. Since we have already chosen the coordinates so that the direction “1” is aligned with the largest eigenvalue and the critical lines can go in both eigen-directions, these two possibilities add up:⁴

$$\frac{\partial \mathcal{L}}{\partial \eta} = \frac{4\sqrt{2}}{(2\pi)^{3/2} \sqrt{1-\gamma^2}} \exp[-\eta^2/2] \int_0^\infty d\tilde{w} \tilde{w} \int_{-\infty}^\infty d\tilde{u} (|2\tilde{w} + \tilde{u}| + |2\tilde{w} - \tilde{u}|) \exp \left[-\frac{(\tilde{u} - \gamma\eta)^2}{2(1-\gamma^2)} - 4\tilde{w}^2 \right]. \quad (27)$$

Note that $|\tilde{w} - \tilde{u}/2| = |\lambda_1| = |\tilde{x}_{11}|$ and $|\tilde{u}/2 + \tilde{w}| = |\lambda_2| = |\tilde{x}_{22}|$. That is, the length of the critical lines per unit volume is given by the average absolute value of the Gaussian curvature of the field in the space orthogonal to the skeleton, given that in stiff approximation the direction of the skeleton is assumed to coincide with the gradient of the field. The reason for this is clear - the higher the curvature, the closer the next neighbouring segment of the skeleton can be, thus increasing the flux *i.e.* the length per unit volume. If we replace $\tilde{w} \rightarrow -\tilde{w}$ in the second integral, we return to the formula (23) with integration over both positive and negative \tilde{w} . The integrated length of the critical lines is reduced to

$$L = \frac{2\sqrt{2}}{\pi} \int_0^\infty \tilde{w} d\tilde{w} \int_{-\infty}^\infty d\tilde{u} (|2\tilde{w} + \tilde{u}| + |2\tilde{w} - \tilde{u}|) \exp \left[-\frac{\tilde{u}^2}{2} - 4\tilde{w}^2 \right]. \quad (28)$$

equations (27) and (28) are the results of the stiff approximation for the threshold dependent differential and the integrated lengths of the critical lines in 2D respectively.

3.2 Primary critical lines in 2D: Skeleton and anti-Skeleton.

The local skeleton is the subset of all the critical lines, which includes the parts that appear as the ridges in the field profile, rather than the valleys. This subset is described by the constraints that the skeleton lines should go along the largest eigenvalue λ_1 and, in addition, that this direction has the smallest curvature, $|\lambda_1| \leq |\lambda_2|$. The anti-skeleton is a mirror structure describing the valley of the field and in all the results can be obtained by replacing $\eta \rightarrow -\eta$ in the formulae for the skeleton.

To derive the expression for the skeleton differential length let us return to equation (27). The critical lines with $\nabla \rho$ aligned with the largest eigenvalue direction have $\tilde{x}_2 = 0$. Thus, only one term is selected by the δ_D -function: it is $\propto 2|\lambda_2| = |2\tilde{w} + \tilde{u}|$. The magnitude restrictions translates into $\tilde{u} \geq 0$, thus

$$\frac{\partial \mathcal{L}^{\text{skel}}}{\partial \eta} = \frac{4\sqrt{2}}{(2\pi)^{3/2} \sqrt{1-\gamma^2}} \exp[-\eta^2/2] \int_0^\infty d\tilde{w} \tilde{w} \int_0^\infty d\tilde{u} (2\tilde{w} + \tilde{u}) \exp \left[-\frac{(\tilde{u} - \gamma\eta)^2}{2(1-\gamma^2)} - 4\tilde{w}^2 \right]. \quad (29)$$

This result should not be confused with equation (28), where \tilde{w} is integrated over full range of negative and positive values and which is strictly equivalent to equation (27), counting critical lines aligned both with the lowest and the largest eigen-directions. Performing the last two integrals one obtains for the differential length in closed form

$$\frac{\partial \mathcal{L}^{\text{skel}}}{\partial \eta} = \frac{1}{\sqrt{2\pi}} \exp \left[-\frac{\eta^2}{2} \right] \left[\frac{1}{8} \left(1 + \frac{2}{\sqrt{\pi}} \gamma\eta \right) \left(1 + \text{Erf} \left[\frac{\gamma\eta}{\sqrt{2}\sqrt{1-\gamma^2}} \right] \right) + \frac{\sqrt{1-\gamma^2}}{2\sqrt{2\pi}} \exp \left(-\frac{\gamma^2 \eta^2}{2(1-\gamma^2)} \right) \right], \quad (30)$$

and for the integrated skeleton length⁵

$$L^{\text{skel}} = \frac{1}{8} + \frac{\sqrt{2}}{4\pi} = 0.23754 (\times R_*^{-1}). \quad (31)$$

Note that modulo the stiff approximation, equation (31) gives a universal, spectral parameter independent, scaling. Figure 3 demonstrates the threshold behaviour of the differential lengths for several values of the spectral parameter γ .

The most important and robust result of our theory is the behaviour of the differential length at high density thresholds

$$\frac{\partial \mathcal{L}^{\text{skel}}}{\partial \eta} \underset{\gamma\eta \rightarrow \infty}{\sim} \frac{1}{\sqrt{2\pi}} \exp \left[-\frac{\eta^2}{2} \right] \times \frac{1}{4} \left(1 + \frac{2}{\sqrt{\pi}} \gamma\eta \right), \quad (32)$$

It represents a bias similar to the one found in Kaiser (1984) for the clustering of high critical points - maxima. According to the latter, the number density of peaks in regions above high thresholds is higher than on average. Similarly, the length density of critical lines above high threshold is enhanced relative to the mean. From the point of view of measurements, perhaps a

⁴ If we do not sort the eigenvalues and, thus, do not restrict the \tilde{w} to be non-negative, then the notions of first and second direction are undefined, and we could choose now that the skeleton goes in, say, the first direction and $\tilde{x}_2 = 0$. We will loose here factor of two which is recovered by having to extend \tilde{w} integration to negative values

⁵ In other words, one expect to find one segment of skeleton per linear section of $\approx (4.2R_*)$.

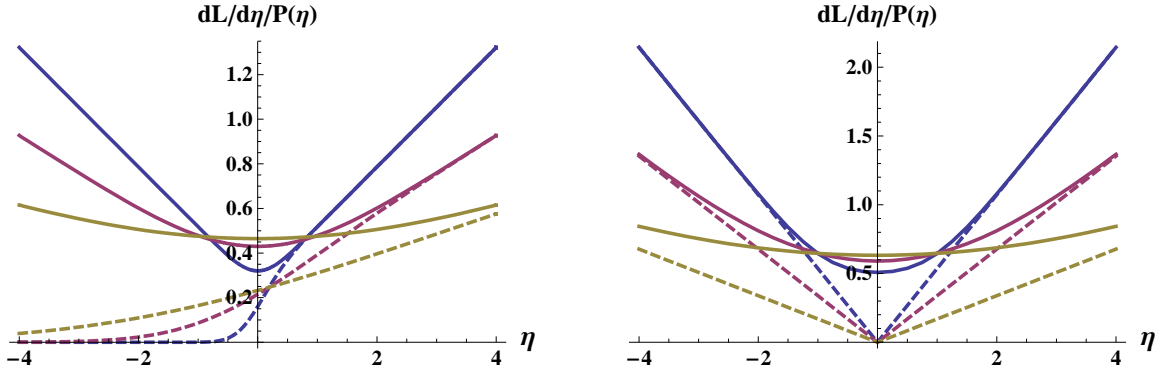


Figure 3. *left:* $\partial\mathcal{L}^{\text{skel}}/\partial\eta/P(\eta)$ (dashed) and $\partial\mathcal{L}^{\text{skel+antiskel}}/\partial\eta/P(\eta)$ (solid) in 2D for the spectral parameter values $\gamma = 0.3, 0.6, 0.95$. *Right:* $\partial\mathcal{L}/\partial\eta/P(\eta)$ (solid) and its asymptotic behaviour (dashed) in 2D for the same spectral parameter values

more interesting quantity than the differential length is the length per unit volume within the regions of high excursions of the field $\mathcal{L}(> \eta)$. In terms of the cumulative length given by equation (9), $\mathcal{L}(> \eta) = L - \mathcal{L}(\eta)$. Its asymptotic behaviour at high η for the skeleton is found by direct integration of equation (32)

$$\mathcal{L}^{\text{skel}}(> \eta) \sim \frac{1}{2} \text{Erfc} \left(\frac{\eta}{\sqrt{2}} \right) \times \frac{1}{4} \left(1 + \frac{2}{\sqrt{\pi}} \gamma \eta \right). \quad (33)$$

The first factor here is the fractional volume occupied by these high excursions of the field. Note that, at large η the differential length divided by the PDF scales like $\eta\gamma/R_* = \eta/R_0$ once the proper scaling with $1/R_*$ is introduced. Hence the differential length as a function of η together with the total length give access to two characteristic scales R_0 and R_* . See Appendix A for a general proof of this result in N dimensions.

The threshold dependence of the statistics of critical lines in the stiff approximation is determined solely by the spectral parameter γ . In the limit $\gamma = 0$, when the distribution of the second derivatives of the field ρ is completely independent on the threshold, the length of the skeleton per unit volume within the regions with ρ/σ_0 in the interval $\eta, \eta + d\eta$ is just proportional to the fraction of the unit volume that these regions occupy. Completely generally, for any type of critical line,

$$\frac{\partial\mathcal{L}}{\partial\eta}(\gamma = 0) = \frac{L}{\sqrt{2\pi}} \exp \left[-\frac{\eta^2}{2} \right]. \quad (34)$$

When $\gamma \rightarrow 1$ the trace of the Hessian u becomes uniquely determined by the field level η (recall equation (6)). For over-dense regions with positive η equation (32) is exact for $\gamma = 1$, while no skeleton exists in under-dense regions in this limit.

Near zero (mean density) threshold the dependence of $\partial\mathcal{L}^{\text{skel}}/\partial\eta$ is

$$\frac{\partial\mathcal{L}^{\text{skel}}}{\partial\eta} \underset{\eta \rightarrow 0}{\sim} \frac{1}{\sqrt{2\pi}} \exp \left[-\frac{\eta^2}{2} \right] \times \frac{1}{4} \left(\frac{1}{2} + \frac{\sqrt{2}\sqrt{1-\gamma^2}}{\pi} + \frac{1}{\sqrt{\pi}} \frac{1 + \sqrt{1-\gamma^2}}{\sqrt{1-\gamma^2}} \gamma \eta \right). \quad (35)$$

Its details, in particular a step-like cutoff at negative η when $\gamma \rightarrow 1$, are sensitive to the definition of the primary lines. In under-dense regions with large negative densities the skeleton is exponentially suppressed.

Starting from equation (30) with $\eta \rightarrow -\eta$ for anti-skeleton, we obtain for the union of both primary critical lines

$$\frac{\partial\mathcal{L}^{\text{skel+antiskel}}}{\partial\eta} = \frac{1}{\sqrt{2\pi}} \exp \left[-\frac{\eta^2}{2} \right] \left[\frac{1}{4} + \frac{1}{2\sqrt{\pi}} \text{Erf} \left(\frac{\gamma\eta}{\sqrt{2}\sqrt{1-\gamma^2}} \right) \gamma \eta + \frac{\sqrt{1-\gamma^2}}{\sqrt{2\pi}} \exp \left(-\frac{\gamma^2\eta^2}{2(1-\gamma^2)} \right) \right], \quad (36)$$

with twice the integrated length

$$L^{\text{skel+antiskel}} = \frac{1}{4} + \frac{1}{\sqrt{2\pi}} = 0.47508 \quad (\times R_*^{-1}) \quad . \quad (37)$$

This function is now symmetric in η with the skeleton providing the dominant contribution described by equation (32) in over-dense regions of space, and the anti-skeleton dominating the under-dense regions. Near the mean, zero, threshold of the field, both critical lines are present

$$\frac{\partial\mathcal{L}^{\text{skel+antiskel}}}{\partial\eta} \underset{\eta \rightarrow 0}{\sim} \frac{1}{\sqrt{2\pi}} \exp \left[-\frac{\eta^2}{2} \right] \left(\frac{1}{4} + \frac{\sqrt{1-\gamma^2}}{\sqrt{2\pi}} + \frac{\gamma^2\eta^2}{2\sqrt{2\pi}\sqrt{1-\gamma^2}} \right). \quad (38)$$

3.3 Secondary critical lines in 2D

Secondary critical lines do not allow for a full analytical treatment and are investigated in Appendix B. They are particularly important near zero threshold, since at this transitional regime the exact behaviour of primary or secondary lines depends

significantly on our somewhat arbitrary separation of the critical lines in types. In this paper we are tracking the skeleton — density ridges — as primary lines emanating from the maxima, until the largest eigenvalue ceases to be the shallowest. Alternative definition may, for example, somewhat extend the skeleton at the expense of secondary lines at lower densities as long as all the eigenvalues transverse to the gradient are negative, i.e until λ_2 becomes positive. As an advantage, the differential length of the skeleton and the corresponding secondary lines defined this way would not exhibit inflections at low densities that can be seen in Figures 3 and B1 for high γ 's. But the downside is that then one loses the ability to describe the primary lines analytically in a closed form. At the high density excursions the properties of the skeleton remain robust with respect to the variations in their exact definition.

However the important advantage of the definition of the primary lines adopted in this paper lies deeper. The magnitude of the eigenvalue along the direction transverse to the gradient is connected to the stability of these trajectories near the critical lines and to their possible bifurcations. This is discussed in part in Section 5.3.

Let us summarize the results for the total set of critical lines, primary and secondary combined, which are, of course, universal whatever the definition of the separate types. Summing up the results of this Section with the corresponding ones in Appendix B

$$L = \frac{\sqrt{2} + \text{acot}(\sqrt{2})}{\pi} = 0.646071 (\times R_*^{-1}). \quad (39)$$

$$\frac{\partial \mathcal{L}}{\partial \eta} \underset{\eta \rightarrow \infty}{\sim} \frac{1}{\sqrt{2\pi}} \exp\left[-\frac{\eta^2}{2}\right] \times \frac{\gamma\eta}{\sqrt{\pi}}, \quad (40)$$

$$\frac{\partial \mathcal{L}}{\partial \eta} \underset{\eta \rightarrow 0}{\sim} \frac{1}{\sqrt{2\pi}} \exp\left[-\frac{\eta^2}{2}\right] \times \left(\frac{\sqrt{2(1-\gamma^2)} + \text{acot}\left(\sqrt{2(1-\gamma^2)}\right)}{\pi} + \frac{\sqrt{2(1-\gamma^2)}}{\pi(3-2\gamma^2)}(\gamma\eta)^2 \right). \quad (41)$$

The full behaviour of the total differential length is presented in Figure 3. One should note the linear asymptotic behaviour at high density levels and the regular quadratic behaviour near zero density threshold⁶. Finally recall that in the section 3 we have omitted almost everywhere a $1/R_*$ factor for the quoted lengths and differential lengths.

4 CRITICAL LINES OF 3D FIELDS

In three dimensions, we carry the computations directly in the eigenframe of the Hessian, following closely the derivation of Sections 3.1 and 3.2. We present the formalism first for all the critical lines and then narrow our focus to the primary ones.

4.1 The length of the critical lines of 3D fields

In 3D, let us use the variables $\tilde{u} = -(\lambda_1 + \lambda_2 + \lambda_3)$, $\tilde{w} = (\lambda_1 - \lambda_3)/2$, $\tilde{v} = (2\lambda_2 - \lambda_1 - \lambda_3)/2$. In the Hessian eigenframe

$$\tilde{s}^1 = (\lambda_2 - \lambda_3)\tilde{x}_2\tilde{x}_3 = (\tilde{w} + \tilde{v})\tilde{x}_2\tilde{x}_3, \quad \tilde{s}^2 = (\lambda_3 - \lambda_1)\tilde{x}_1\tilde{x}_3 = -2\tilde{w}\tilde{x}_1\tilde{x}_3, \quad \tilde{s}^3 = (\lambda_1 - \lambda_2)\tilde{x}_1\tilde{x}_2 = (\tilde{w} - \tilde{v})\tilde{x}_1\tilde{x}_2, \quad (43)$$

and

$$\begin{aligned} \widetilde{\nabla s^1} &= \{0, \lambda_2(\lambda_2 - \lambda_3)\tilde{x}_3, \lambda_3(\lambda_2 - \lambda_3)\tilde{x}_2\} = \left\{0, -\frac{1}{3}(\tilde{u} - 2\tilde{v})(\tilde{w} + \tilde{v})\tilde{x}_3, -\frac{1}{3}(\tilde{u} + \tilde{v} + 3\tilde{w})(\tilde{w} + \tilde{v})\tilde{x}_2\right\}, \\ \widetilde{\nabla s^2} &= \{\lambda_1(\lambda_3 - \lambda_1)\tilde{x}_3, 0, \lambda_3(\lambda_3 - \lambda_1)\tilde{x}_1\} = \left\{\frac{2}{3}(\tilde{u} + \tilde{v} - 3\tilde{w})\tilde{w}\tilde{x}_3, 0, \frac{2}{3}(\tilde{u} + \tilde{v} + 3\tilde{w})\tilde{w}\tilde{x}_1\right\}, \\ \widetilde{\nabla s^3} &= \{\lambda_1(\lambda_1 - \lambda_2)\tilde{x}_2, \lambda_2(\lambda_1 - \lambda_2)\tilde{x}_1, 0\} = \left\{-\frac{1}{3}(\tilde{u} + \tilde{v} - 3\tilde{w})(\tilde{w} - \tilde{v})\tilde{x}_2, -\frac{1}{3}(\tilde{u} - 2\tilde{v})(\tilde{w} - \tilde{v})\tilde{x}_3, 0\right\}. \end{aligned} \quad (44)$$

In the eigenvalue space the measure is $2\pi^2|(\lambda_1 - \lambda_2)(\lambda_2 - \lambda_3)(\lambda_3 - \lambda_1)|$ and the eigenvalues are considered sorted. For sorted eigenvalues the choice of the directions has been fixed and the (s^2, s^3) , (s^1, s^3) and (s^1, s^2) pairs of surfaces describe different possibilities for the critical line. Those choices add together in the average integrated length. Using the variable \tilde{w}, \tilde{v} the condition of eigenvalues being sorted is $\tilde{w} \geq 0$, $-\tilde{w} \leq \tilde{v} \leq \tilde{w}$.

Let us consider the critical lines that are the intersections of (s^2, s^3) . Their differential length is given by

$$\begin{aligned} \frac{\partial \mathcal{L}}{\partial \eta} &= 2\pi^2 \cdot \frac{3}{2} \cdot \frac{3^{3/2}15^{5/2}}{(2\pi)^5\sqrt{1-\gamma^2}} \exp\left[-\frac{1}{2}\eta^2\right] \int |(\lambda_1 - \lambda_2)(\lambda_2 - \lambda_3)(\lambda_3 - \lambda_1)| d\lambda_1 d\lambda_2 d\lambda_3 d\tilde{x}_1 d\tilde{x}_2 d\tilde{x}_3 \left| \widetilde{\nabla s^2} \times \widetilde{\nabla s^3} \right| \delta_D(\tilde{s}^2) \delta_D(\tilde{s}^3) \\ &\quad \times \exp\left[-\frac{(\tilde{u} - \gamma\eta)^2}{2(1-\gamma^2)} - \frac{15}{2}\tilde{w}^2 - \frac{5}{2}\tilde{v}^2 - \frac{3}{2}\tilde{x}_1^2 - \frac{3}{2}\tilde{x}_2^2 - \frac{3}{2}\tilde{x}_3^2\right]. \end{aligned} \quad (45)$$

⁶ For all γ but $\gamma = 1$, for which

$$\frac{\partial \mathcal{L}}{\partial \eta}(\gamma \rightarrow 1, \eta \rightarrow 0) \sim \frac{1}{\sqrt{2\pi}} \exp[-\eta^2/2] \left(\frac{1}{2} + \frac{1}{3\sqrt{\pi}}|\eta|^3 - \frac{1}{10\sqrt{\pi}}|\eta|^5 \dots \right). \quad (42)$$

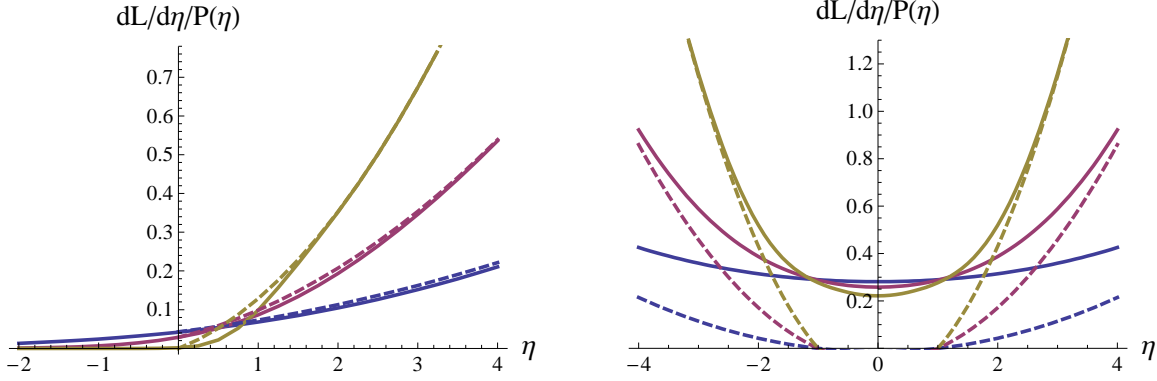


Figure 4. *Left:* The skeleton $\partial\mathcal{L}^{\text{skel}}/\partial\eta/P(\eta)$ (solid) and its asymptotic behaviour at high density thresholds (dashed) in 3D. The anti-skeleton is described by the curves symmetric with respect to a reflection of η . *Right:* $\partial\mathcal{L}/\partial\eta/P(\eta)$ its asymptotic behaviour for the total set of critical lines. The spectral parameter values are (from bottom to top at high η) $\gamma = 0.3, 0.6, 0.95$.

Integration over $\delta_D(\tilde{s}_2)$ and $\delta_D(\tilde{s}_3)$ leads to the only possibility $\tilde{x}_2 = 0, \tilde{x}_3 = 0$. That is, the choice of the surface S_2 and S_3 in the Hessian eigenframe describes the skeleton along which the gradient is aligned with the direction 1, correspondent to the largest eigenvalue, while in the directions 2 and 3 the components of the gradient of the field vanish. With $\tilde{x}_2 = \tilde{x}_3 = 0$ we get a simple expression for

$$\left| \widetilde{\nabla}_{S_2} \times \widetilde{\nabla}_{S_3} \right| = |\lambda_2 \lambda_3 (\lambda_3 - \lambda_1) (\lambda_1 - \lambda_2)| \tilde{x}_1^2 = \frac{2}{9} |(\tilde{u} - 2\tilde{v})(\tilde{u} + \tilde{v} + 3\tilde{w})(\tilde{w} - \tilde{v})\tilde{w}| \tilde{x}_1^2, \quad (46)$$

while the subsequent integration over \tilde{x}_2 and \tilde{x}_3 using δ_D -functions and afterwards over \tilde{x}_1 gives

$$\frac{\partial\mathcal{L}^1}{\partial\eta} = \frac{3^3 5^{5/2}}{16\pi^2 \sqrt{2\pi(1-\gamma^2)}} \exp\left[-\frac{1}{2}\eta^2\right] \int d\lambda_1 d\lambda_2 d\lambda_3 (\lambda_1 - \lambda_2)(\lambda_2 - \lambda_3)(\lambda_3 - \lambda_1) |\lambda_2 \lambda_3| \exp\left[-\frac{(\tilde{u} - \gamma\eta)^2}{2(1-\gamma^2)} - \frac{15}{2}\tilde{w}^2 - \frac{5}{2}\tilde{v}^2\right]. \quad (47)$$

Notice again that what the integrand involves the Gaussian curvature in the direction orthogonal to the gradient, which in stiff approximation is the direction of the filament itself. The contributions of the critical lines directed along the second and third eigen-direction is given by similar considerations and are added together when all critical lines are considered. Changing variables one finally obtains

$$\frac{\partial\mathcal{L}}{\partial\eta} = \frac{3^3 5^{5/2} \exp[\eta^2/2]}{4\pi^2 \sqrt{2\pi(1-\gamma^2)}} \int d\tilde{u} d\tilde{w} d\tilde{v} \tilde{w}(\tilde{w}^2 - \tilde{v}^2) (|\lambda_2 \lambda_3| + |\lambda_1 \lambda_3| + |\lambda_1 \lambda_2|) \exp\left[-\frac{(\tilde{u} - \gamma\eta)^2}{2(1-\gamma^2)} - \frac{15}{2}\tilde{w}^2 - \frac{5}{2}\tilde{v}^2\right], \quad (48)$$

while the integrated length is

$$L = \frac{3^3 5^{5/2}}{4\pi^2} \int d\tilde{u} d\tilde{w} d\tilde{v} \tilde{w}(\tilde{w}^2 - \tilde{v}^2) (|\lambda_2 \lambda_3| + |\lambda_1 \lambda_3| + |\lambda_1 \lambda_2|) \exp\left[-\frac{1}{2}\tilde{u}^2 - \frac{15}{2}\tilde{w}^2 - \frac{5}{2}\tilde{v}^2\right], \quad (49)$$

with ⁷

$$|\lambda_2 \lambda_3| + |\lambda_1 \lambda_3| + |\lambda_1 \lambda_2| = \frac{1}{9} [|(\tilde{u} - 2\tilde{v})(\tilde{u} + \tilde{v} + 3\tilde{w})| + |(\tilde{u} + \tilde{v} + 3\tilde{w})(\tilde{u} + \tilde{v} - 3\tilde{w})| + |(\tilde{u} - 2\tilde{v})(\tilde{u} + \tilde{v} - 3\tilde{w})|]. \quad (50)$$

The equations (48) and (49) account for all the critical lines. In Figure 4 (right panel) the results for 3D critical lines are plotted while the discussion of the corresponding asymptotics is given in the Appendix C. We shall now turn our attention to the study of the primary lines and, in particular, the 3D skeleton that delineates the over dense filamentary structure and is of more direct observational interest.

4.2 Primary critical lines of 3D fields: Skeleton and Anti-Skeleton

The subset of critical lines identified with the skeleton correspond to the lines with the gradient aligned with the largest eigenvalue λ_1 while having $\lambda_1 + \lambda_2 \leq 0$. In equation (48) such lines are described by the first term $\sim |\lambda_2 \lambda_3|$. The differential

⁷ One should note the correspondence with the well-known result for the number density of extrema of the field (Bardeen et al. 1986)

$$N_{\text{ext}} \propto \int d\tilde{u} d\tilde{w} d\tilde{v} \tilde{w}(\tilde{w}^2 - \tilde{v}^2) |\lambda_1 \lambda_2 \lambda_3| \exp\left[-\frac{1}{2}\tilde{u}^2 - \frac{15}{2}\tilde{w}^2 - \frac{5}{2}\tilde{v}^2\right].$$

which is determined by the mean three-dimensional Gaussian curvature $|\lambda_1 \lambda_2 \lambda_3|$.

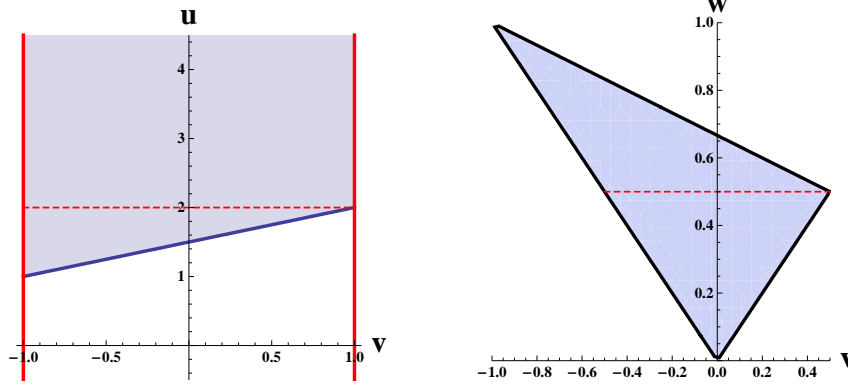


Figure 5. *Left:* Integration zones in the \tilde{v}, \tilde{u} plane for the 3D skeleton analysis. Variables are given in units of \tilde{w} . \tilde{v} varies from $-\tilde{w}$ to $+\tilde{w}$, while \tilde{u} must be greater than $\frac{1}{2}(\tilde{v} + 3\tilde{w})$. In the allowed shaded region $0 > \lambda_2 \geq \lambda_3$ everywhere. Horizontal lines mark the further subdivision of the integration space if the order of integration is changed according to equation (53). *Right:* Integration zones in the (\tilde{v}, \tilde{w}) plane after \tilde{u} has been mapped to the $[0 - \infty]$ interval. Variables are given in the units of \tilde{u} . The lower triangular zone corresponds to the semi-open rectangular band above the red dashed line in the left panel. In this region the integrand is given by the first term of equation (53). It dominates the high η asymptotics.

length of the skeleton is then

$$\begin{aligned} \frac{\partial \mathcal{L}^{\text{skel}}}{\partial \eta} &= \frac{3^3 5^{5/2} \exp[-\eta^2/2]}{4\pi^2 \sqrt{2\pi(1-\gamma^2)}} \int_0^\infty d\tilde{w} \int_{-\tilde{w}}^{\tilde{w}} d\tilde{v} \int_{\frac{1}{2}(\tilde{v}+3\tilde{w})}^\infty d\tilde{u} \tilde{w}(\tilde{w}^2 - \tilde{v}^2) \lambda_2 \lambda_3 \exp\left[-\frac{(\tilde{u} - \gamma\eta)^2}{2(1-\gamma^2)} - \frac{15}{2}\tilde{w}^2 - \frac{5}{2}\tilde{v}^2\right], \\ &= \frac{3 \cdot 5^{5/2} \exp[-\eta^2/2]}{4\pi^2 \sqrt{2\pi(1-\gamma^2)}} \int_0^\infty d\tilde{w} \int_{-\tilde{w}}^{\tilde{w}} d\tilde{v} \int_{\frac{1}{2}(\tilde{v}+3\tilde{w})}^\infty d\tilde{u} \tilde{w}(\tilde{w}^2 - \tilde{v}^2)(\tilde{u} - 2\tilde{v})(\tilde{u} + \tilde{v} + 3\tilde{w}) \exp\left[-\frac{(\tilde{u} - \gamma\eta)^2}{2(1-\gamma^2)} - \frac{15}{2}\tilde{w}^2 - \frac{5}{2}\tilde{v}^2\right]. \end{aligned} \quad (51)$$

The integration in $\tilde{v}-\tilde{u}$ plane is limited to the region $\tilde{u} > \frac{1}{2}(\tilde{v} + 3\tilde{w})$, as shown in the left panel of Figure 5. The integrated length of the skeleton is

$$L^{\text{skel}} = 0.046186 (\times R_*^{-2}), \quad (52)$$

that is, one expect on average one skeleton line crossing a random $\approx (5R_*)^2$ surface element. The results of integration of equation (51) are presented in the left panel of Figure 4.

4.2.1 Asymptotic behaviour at $\gamma\eta \rightarrow \infty$

To study high η asymptotes it is useful to change the order of integration to have the \tilde{u} integral as the outmost one. The inner integration in $\tilde{v}-\tilde{w}$ plane is then carried out over the region shown in the right panel of Figure 5.

$$\int_0^\infty d\tilde{w} \int_{-\tilde{w}}^{\tilde{w}} d\tilde{v} \int_{\frac{1}{2}(\tilde{v}+3\tilde{w})}^\infty d\tilde{u} \rightarrow \int_0^\infty d\tilde{u} \int_0^{\tilde{u}/2} d\tilde{w} \int_{-\tilde{w}}^{\tilde{w}} d\tilde{v} + \int_0^\infty d\tilde{u} \int_{\tilde{u}/2}^{\tilde{u}} d\tilde{w} \int_{-\tilde{w}}^{2\tilde{u}-3\tilde{w}} d\tilde{v} \quad (53)$$

The last term is exponentially suppressed as $\eta \rightarrow \infty$ while the first one gives

$$\begin{aligned} \frac{\partial \mathcal{L}^{\text{skel}}}{\partial \eta} &\underset{\gamma\eta \rightarrow \infty}{\sim} \frac{3 \cdot 5^{5/2} \exp[-\eta^2/2]}{4\pi^2 \sqrt{2\pi(1-\gamma^2)}} \int_0^\infty d\tilde{u} \int_0^{\tilde{u}/2} d\tilde{w} \int_{-\tilde{w}}^{\tilde{w}} d\tilde{v} \tilde{w}(\tilde{w}^2 - \tilde{v}^2)(\tilde{u} - 2\tilde{v})(\tilde{u} + \tilde{v} + 3\tilde{w}) \exp\left[-\frac{(\tilde{u} - \gamma\eta)^2}{2(1-\gamma^2)} - \frac{15}{2}\tilde{w}^2 - \frac{5}{2}\tilde{v}^2\right] \\ &\underset{\gamma\eta \rightarrow \infty}{\sim} \frac{1}{\sqrt{2\pi}} \exp\left[-\frac{1}{2}\eta^2\right] \frac{(\gamma\eta)^2 + 9(\gamma\eta)/\sqrt{10\pi} + (9/10 - \gamma^2)}{6\pi}. \end{aligned} \quad (54)$$

The leading quadratic and the next linear terms can be recovered found by replacing $\tilde{u} \rightarrow \gamma\eta$ in the pre-exponential factor and treating the exponent as the δ_{D} -function. A more detailed asymptotic study of this Laplace-type integral is required to recover the third-order constant term, that also contributes to the accuracy of the expansion at the level demonstrated in Figure 4.

One finds that in the leading order in η the skeleton has the differential length growing as $(\gamma\eta)^2$ (see also Appendix A) and involves, as expected, a third of all the critical lines (compare with Appendix C) in the regions of high excursions concentrated around the maxima of the field. However, at intermediated thresholds, the skeleton constitutes more than a half of all critical lines, highlighting enhanced importance of the filamentary dense ridges among other critical lines.⁸

⁸ Note the appearance of the linear in $\gamma\eta$ term in the next to leading order for the skeleton, that canceled out for the critical lines.

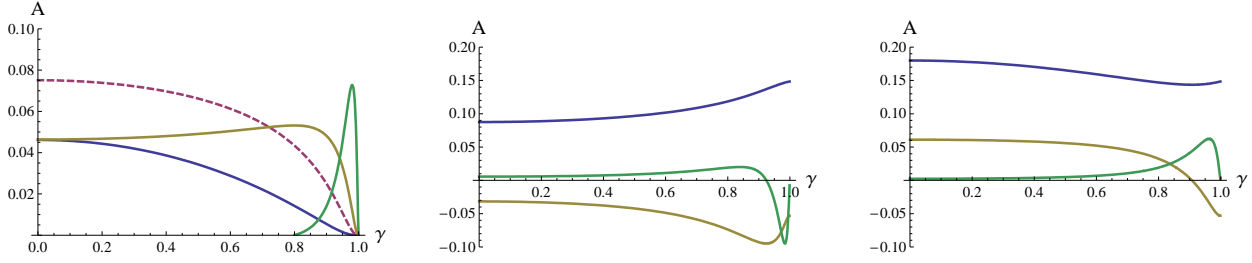


Figure 6. First coefficients of low- η power expansion (A_0 – blue, A_2 – yellow, A_4 – green) of the differential lengths of the 3D skeleton (left), inter-skeleton (middle) and total set of primary critical lines (right). The odd terms (e.g. A_1 – dashed) are present only for the asymmetric case of the primary lines.

4.2.2 Power series at $\eta \rightarrow 0$ and Hermite expansion

Using two alternative series representations of the shifted Gaussian form that encodes the dependence of the skeleton on the threshold η

$$\frac{1}{\sqrt{2\pi(1-\gamma^2)}} \exp\left[-\frac{(u-\gamma\eta)^2}{2(1-\gamma^2)}\right] = \frac{1}{\sqrt{2\pi}} \exp\left[-\frac{u^2}{2}\right] \sum_{k=0}^{\infty} \gamma^k H_k(\eta) H_k(u), \quad (55)$$

$$= \frac{1}{\sqrt{2\pi(1-\gamma^2)}} \exp\left[-\frac{u^2}{2(1-\gamma^2)}\right] \sum_{k=0}^{\infty} \frac{1}{\sqrt{k!}} \left(\frac{\gamma}{\sqrt{1-\gamma^2}}\eta\right)^k H_k\left(\frac{u}{\sqrt{1-\gamma^2}}\right), \quad (56)$$

we obtain either power series or Hermite⁹ (Novikov et al. 2006) expansion of the differential length

$$\frac{\partial \mathcal{L}^{\text{skel}}}{\partial \eta} = \frac{1}{\sqrt{2\pi}} \exp[-\eta^2/2] \times \begin{cases} \sum_{k=0}^{\infty} A_k(\gamma)(\gamma\eta)^k, \\ \sum_{k=0}^{\infty} B_k \gamma^k H_k(\eta), \end{cases} \quad (57)$$

where

$$A_k(\gamma) \equiv \frac{3 \cdot 5^{5/2}}{4\pi^2 \sqrt{k!} (1-\gamma^2)^{\frac{k+1}{2}}} \int_0^{\infty} d\tilde{w} \int_{-\tilde{w}}^{\tilde{w}} d\tilde{v} \int_{\frac{1}{2}(\tilde{v}+3\tilde{w})}^{\infty} d\tilde{u} \tilde{w}(\tilde{w}^2 - \tilde{v}^2)(\tilde{u} - 2\tilde{v})(\tilde{u} + \tilde{v} + 3\tilde{w}) \\ \times \exp\left[-\frac{\tilde{u}^2}{2(1-\gamma^2)} - \frac{15}{2}\tilde{w}^2 - \frac{5}{2}\tilde{v}^2\right] H_k\left(\frac{\tilde{u}}{\sqrt{1-\gamma^2}}\right), \quad (58)$$

and

$$B_k \equiv \frac{3 \cdot 5^{5/2}}{4\pi^2} \int_0^{\infty} d\tilde{w} \int_{-\tilde{w}}^{\tilde{w}} d\tilde{v} \int_{\frac{1}{2}(\tilde{v}+3\tilde{w})}^{\infty} d\tilde{u} \tilde{w}(\tilde{w}^2 - \tilde{v}^2)(\tilde{u} - 2\tilde{v})(\tilde{u} + \tilde{v} + 3\tilde{w}) \exp\left[-\frac{\tilde{u}^2}{2} - \frac{15}{2}\tilde{w}^2 - \frac{5}{2}\tilde{v}^2\right] H_k(\tilde{u}) \quad (59)$$

These two expansions are similar but distinct. The power-law expansion is suitable for an accurate analysis of the differential length near zero threshold for all $\gamma < 1$. On the other hand, the expansion in orthogonal Hermite polynomials is useful as an approximation over an extended range of thresholds. Both series are improper for $\gamma = 1$.

Although these coefficients can be computed analytically, their expressions are too cumbersome. Instead, we plot several leading ones in Figure 6. Remarkably, the power in Hermite expansion is concentrated in a few low order terms, in particular, $k = 0, 1, 2, 3$ for the skeleton, with subsequent terms forming a slowly decaying oscillating series. This finding confirms in 3D the conjecture of Novikov et al. (2006). The contribution of the first three most dominant terms, $\sum_{k=0}^2 B_k H_k(\eta) = 0.0462 + 0.0751\gamma\eta + 0.0464\gamma^2(\eta^2 - 1)$ has the same structure and remarkably similar coefficients as the high η asymptotics of equation (54) which evaluates to $0.0477 + 0.0852\gamma\eta + 0.0531\gamma^2(\eta^2 - 1)$. This explains why the high η asymptotics provides a visually good fit through all thresholds when γ is not too high. At $\gamma \rightarrow 1$, the oscillatory tail of Hermite series provides the correction that reflects the irregular nature of the expansion in this limit.

The power series expansion reflects the features of the Hermite expansion. Starting, by definition, at $A_0(0) = B_0 = \mathcal{L}_{\text{tot}}^{\text{skel}} = 0.0462$, A_0 behaves as $A_0(\gamma) \approx \mathcal{L}_{\text{tot}}(1-\gamma^2)$ over most of the γ range. Coupled with $A_2(\gamma) \approx \text{const} = \mathcal{L}_{\text{tot}}$ and $A_1(\gamma) \approx 0.0751\sqrt{1-\gamma^2}$ we get for the first three orders $\sum_{k=0}^2 A_k(\gamma)(\gamma\eta)^k \approx 0.0462 + 0.0751\sqrt{1-\gamma^2}\gamma\eta + 0.0462\gamma^2(\eta^2 - 1)$, close both to the Hermite expansion and to the high η law for moderate γ . On the other hand, the power series expansion explicitly demonstrates the increasing importance of higher-order terms for $\gamma > 0.8$.

⁹ we use here the *normalized* Hermite polynomials following probabilistic definition, $1/\sqrt{2\pi} \int_{-\infty}^{\infty} du \exp[-\frac{1}{2}u^2] H_k(u) H_m(u) = \delta_{mk}$

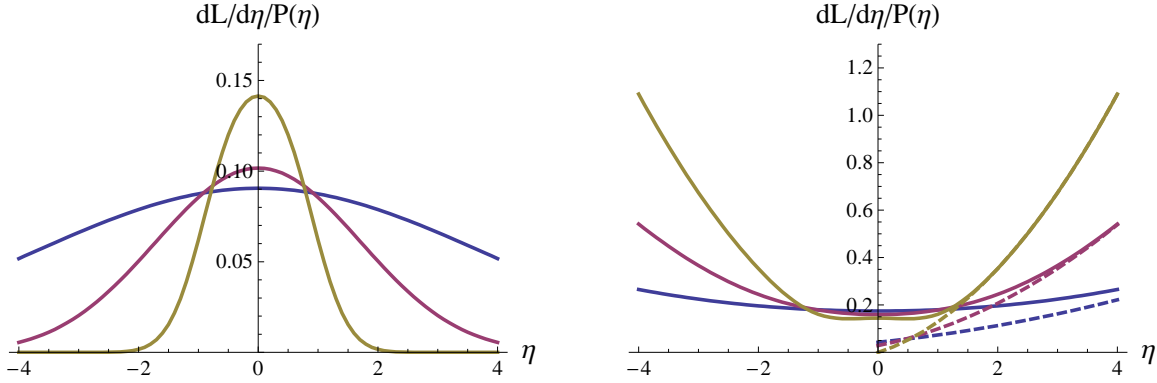


Figure 7. Differential length $\partial\mathcal{L}/\partial\eta/P(\eta)$ of the intermediate (left panel) and combined primary lines (right panel) as function of the threshold η in 3D. Different curves from blue to yellow correspond to the spectral parameter values $\gamma = 0.3, 0.6, 0.95$. The dashed curves, drawn only for positive η , correspond to high- η asymptotic solutions.

4.3 Primary critical lines of 3D fields: Inter-Skeleton and the overall behaviour

The intermediate primary critical lines are associated with saddle-like regions where the largest eigenvalues in magnitude are $\lambda_1 \geq 0$ and $\lambda_3 \leq 0$, and have opposite signs, and the shallowest direction aligned with the gradient is the second one with $-\lambda_1 < \lambda_2 < -\lambda_3$. Their appearance reflects the complexity of critical lines in space of more than two dimensions.

The differential length of the intra-skeleton computed in the stiff approximation is presented in Figure 7. The conditions for intermediate lines are prevalent for the regions of the field of moderate values - within 2σ ($|\eta| < 2$ of the zero mean for $\gamma > 0.6$). Although the occurrence of the intra-skeleton within these regions is never large ($\partial\mathcal{L}/\partial\eta/P(\eta)$ is relatively small), the regions corresponding to a near mean density occupy large fractions of the total volume, and as the result the total length of the intermediate skeleton is almost twice that of the skeleton or the anti-skeleton:

$$L^{\text{inter}} = 0.087533 (\times R_*^{-2}). \quad (60)$$

It constitutes nearly a half of the total length of the primary critical lines

$$L^{\text{prim}} = L^{\text{skel}} + L^{\text{antiskel}} + L^{\text{inter}} = 0.179905 (\times R_*^{-2}). \quad (61)$$

At high $|\eta|$ thresholds, in very dense regions near maxima or under-dense regions near minima of the field, the intermediate skeleton is rare.

The total set of the primary critical line is even more than the skeleton dominated by the low order terms in Hermite expansion. Indeed, Figure 6 demonstrates that just the first two terms (odd orders are absent due to symmetry) in Hermite series are dominant, $\sum_{k=0}^{\infty} B_k H_k(\eta) \approx \mathcal{L}_{\text{tot}}^{\text{prim}} (1 + 0.340\gamma^2(\eta^2 - 1))$.

4.4 Validity of the stiff approximation

Let us consider the opposite to “stiff” regime, when the derivatives of the Hessian dominate the ∇_s ,

$$(\nabla_m s^i)^{\text{Iax}} \approx \tilde{\gamma}^{-1} \sum_{jkl} \epsilon^{ijk} x_{jlm} x_l x_k. \quad (62)$$

Although not natural for cosmology-inspired spectra, such a situation arises when the power spectrum has an extended short wave tail with spectral index¹⁰ n between -9 and -5 . Such spectra have small $\tilde{\gamma}$, $\tilde{R} \ll R_*$ and there are many inflection points of the field per extremum. Interestingly, this regime also automatically means that the correlation between the gradient and third derivatives of the field is small.

Using the Hessian eigenframe formalism, we can obtain the important results without explicit computation of the differential length. Let us focus on the critical lines corresponding to the first eigenvalue. Equations (43) for \mathcal{S} -surfaces gives rise to two δ_D -functions, $\delta_D(2\tilde{w}\tilde{x}_1\tilde{x}_3)\delta_D((\tilde{w} - \tilde{v})\tilde{x}_1\tilde{x}_2)$ that after integration over the transverse gradient components \tilde{x}_2 and \tilde{x}_3 enforce $\tilde{x}_2 = \tilde{x}_3 = 0$, with the Jacobian factor $1/|2\tilde{w}(\tilde{w} - \tilde{v})\tilde{x}_1^2|$. The length element in this frame obeys

$$|\nabla s^2 \times \nabla s^3|^{\text{Iax}} \approx \tilde{\gamma}^{-2} x_1^4 \left| \sum_{ijmn} \epsilon_{kmn} \epsilon^{2i1} \epsilon^{3j1} x_{i1m} x_{j1n} \right| \equiv \tilde{\gamma}^{-2} x_1^4 \psi(x_{klm}), \quad (63)$$

¹⁰ In a cosmological framework this takes place when the density field with $n < -1$ spectrum is smoothed with a top-hat window.

where the last expression defines the $\psi(x_{klm})$ function. The differential length is now given by

$$\frac{\partial \mathcal{L}^{\text{last}}}{\partial \eta} = \frac{1}{\tilde{R}^2} \left\{ \frac{3^3 5^{5/2}}{8\pi^3 \sqrt{1-\gamma^2}} \exp \left[-\frac{1}{2} \eta^2 \right] \int d\tilde{u} d\tilde{w} d\tilde{v} (\tilde{w} + \tilde{v}) \exp \left[-\frac{(\tilde{u} - \gamma\eta)^2}{2(1-\gamma^2)} - \frac{15}{2} \tilde{w}^2 - \frac{5}{2} \tilde{v}^2 \right] \right\} \times \left\{ \int x_1^2 dx_1 d^{10} x_{klm} \psi(x_{klm}) P_1(x_1, x_2 = x_3 = 0, x_{klm}) \right\} \quad (64)$$

The last integral, with P_1 given by equation (D6), is a function of $\tilde{\gamma}$ only. The first term shows that, since the integrand prefactor is independent on \tilde{u} , the differential length does not depend on the threshold η at large η (it does at small η only because of non-trivial integration boundaries dependent on the exact type of critical lines). This is not surprising, since in this limit, there is little link between the skeleton length and the second derivatives, the only ones that are correlated with the field value. Such threshold independent behaviour is not observed in simulations with cosmological spectra, which argues once again for the statistical validity of the “stiff” approximation.

4.5 Measurements

In this section we compare the predictions of the local theory in stiff approximation with the measurements of the statistical properties of the critical lines done on realizations of the Gaussian fields with different power spectra.

We perform the measurements on critical lines found according to the global definition. The measurements are carried as follows: a set (typically ~ 100) of scale-invariant Gaussian random field of a N - D maps (typically 1024^2) or cubes (typically 256^3) is generated with a given power index of $n = 0, -1$ or -2 . The N - D cube is then smoothed via convolution with a Gaussian kernel of width 6 pixels. The spectral parameters, $\gamma, \tilde{\gamma}$ etc... are computed through the second moments of the derivative of the smoothed field. The set of critical lines is then extracted as the intersection of the peak patches and void patches (see Sousbie et al. (2008) for details). In Figure 8 an example realization of the primary critical lines in 3D cube is shown. Since the algorithm produces a set of segments describing those critical lines tagged by the underlying (smoothed) density field, it is straightforward to compute the total and differential length per unit volume of the whole set. The differential length per unit modulus gradient is extracted by tagging the critical lines with this modulus (obtained via Fourier transform differentiation) and proceeding as before. Finally, the curvature of the skeleton is measured by computing the local curvature of a set of adjacent segments via finite difference.

Let us emphasize that these measurements correspond to properties of the global skeleton, whereas the theory developed in this paper is focused on the local skeleton. Hence even more remarkable is the match between the measured and the theoretical differential lengths for all values of γ , that is exhibited in Figure 9. This accuracy should be considered as indicative of the correspondence between the stiff approximation to the local theory and the global set of critical lines.

5 OTHER STATISTICS AND SPECTRAL PARAMETERS

In the previous sections, the emphasis has been on the differential length of the critical lines as a function of the excursion in density. As argued in Sousbie et al. (2008) and demonstrated here, it provides means of constraining the shape parameter, γ . Let us now explore other statistics which will allow us to constraint other shape parameters. In particular, let us demonstrate that the differential length as a function of the excursion in the modulus of the *gradient* of the density and the differential curvature depend on the second shape parameter, $\tilde{\gamma}$. Finally, we investigate the number density of singular points on the critical lines.

5.1 Differential length versus the gradient modulus

The differential length of the skeleton with respect to the threshold η carries information on the spectral parameter γ thanks to the correlation between the value η and the Hessian of the field. In the stiff approximation the Hessian curvature completely determines the length of the critical lines. For the exact formulation, the length also depends on the third derivatives, that are correlated with the first derivatives via the parameter $\tilde{\gamma}$. Thus, measuring length as a function of the modulus of the gradient should carry information on $\tilde{\gamma}$ and provide an estimate of an impact the third derivatives have on the length statistics of the critical lines.

To demonstrate the dependence of the skeleton length on the gradient of the field in “stiff” approximation let us return to equation (45) which we take integrated over all density thresholds. As before, we perform the integration over the δ -functions that enforces alignment of the gradient with the first eigen-direction, $x_2 = x_3 = 0$, however this time we do not integrate over but rather take the differential of the result with respect to x_1 . Noting that $|x_1| = X \equiv \sqrt{x_1^2 + x_2^2 + x_3^2}$, we obtain in place of equation (47)

$$\frac{\partial \mathcal{L}}{\partial X} = \frac{3}{2} \cdot \frac{3^{3/2} 15^2 5^{1/2}}{(2\pi)^{5/2}} \exp \left[-\frac{3}{2} X^2 \right] \int |(\lambda_1 - \lambda_2)(\lambda_2 - \lambda_3)(\lambda_3 - \lambda_1)| d\lambda_1 d\lambda_2 d\lambda_3 |\lambda_2 \lambda_3| \exp \left[-\frac{1}{2} \tilde{u}^2 - \frac{15}{2} \tilde{w}^2 - \frac{5}{2} \tilde{v}^2 \right], \quad (65)$$

where the last integral does not depend on X . Dividing by the integrated length, $L = \int_0^\infty \partial \mathcal{L} / \partial X dX$, and generalizing the

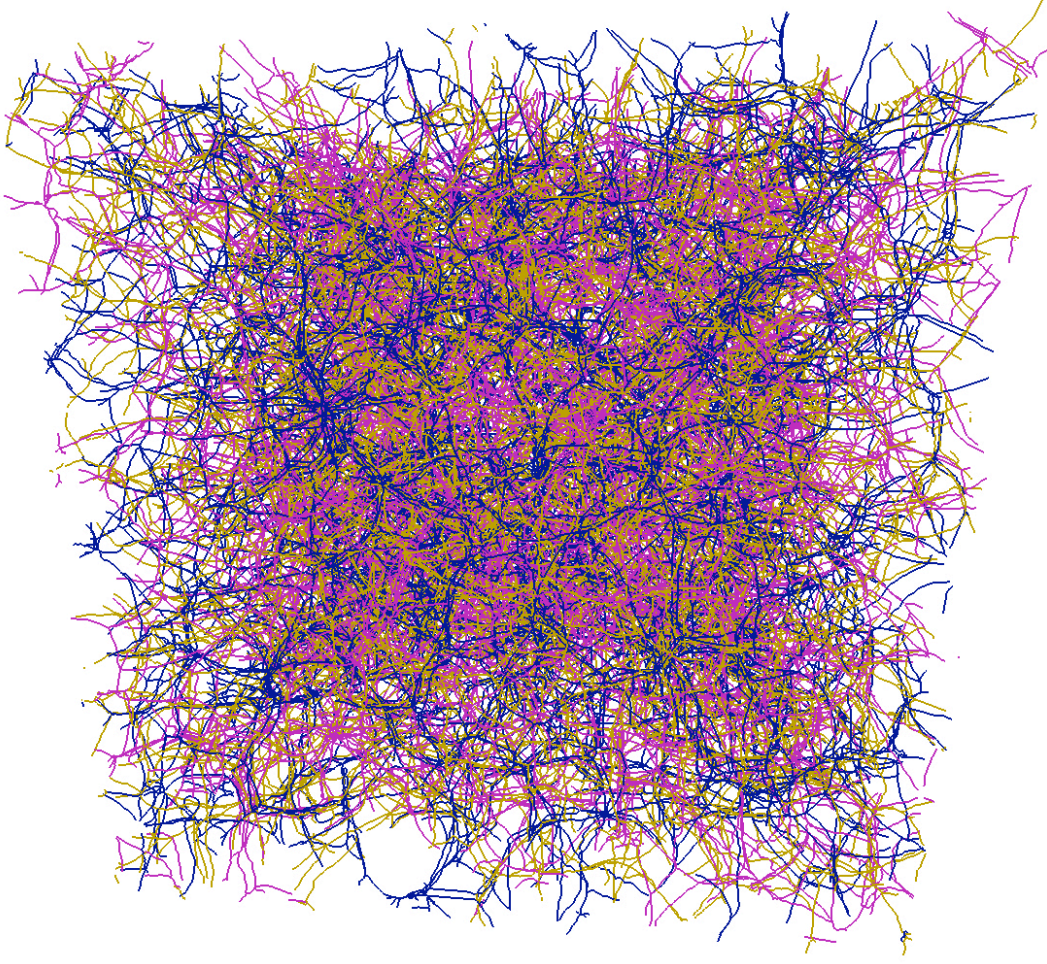


Figure 8. An example of set of primary critical lines (resp. skeleton in blue, intermediate in magenta and anti skeleton in gold) for a scale invariant power spectrum with $\gamma = 0.6$ in a 256^3 box smoothed over 5 pixels.

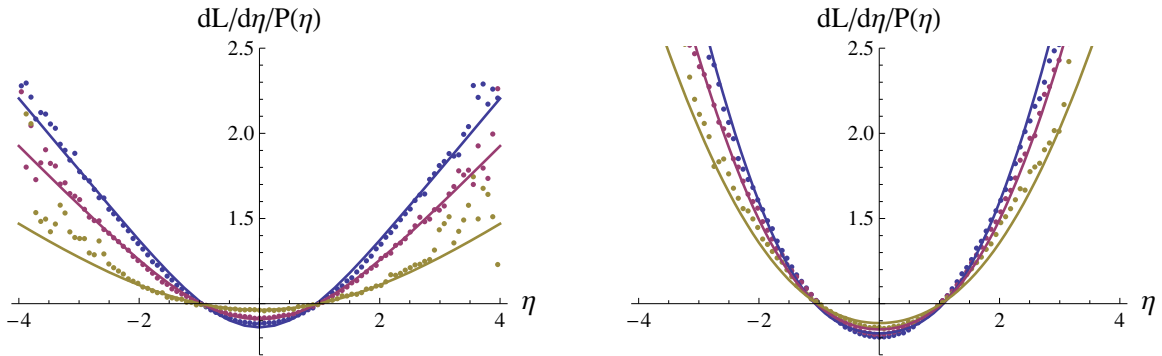


Figure 9. The relative differential length, $\partial\mathcal{L}/\partial\eta/\text{PDF}$, measured in simulation of 2D (*left*) and 3D (*right*) Gaussian random fields with scale invariant power-law spectra versus predictions of the local theory in stiff approximation (solid curves). The spectral parameter $\gamma = 0.71, 0.59, 0.39$ for the 2D and $\gamma = 0.77, 0.70, 0.60$ for the 3D simulations.

result to fields in arbitrary N dimensions we conclude that

$$\left(\frac{1}{L} \frac{\partial\mathcal{L}}{\partial X}\right)^{\text{stiff}} = \sqrt{\frac{2N}{\pi}} \exp\left[-\frac{N}{2} X^2\right]. \quad (66)$$

The exact dependence of the differential lengths will deviate from this form in a $\tilde{\gamma}$ -dependent way. It is natural to

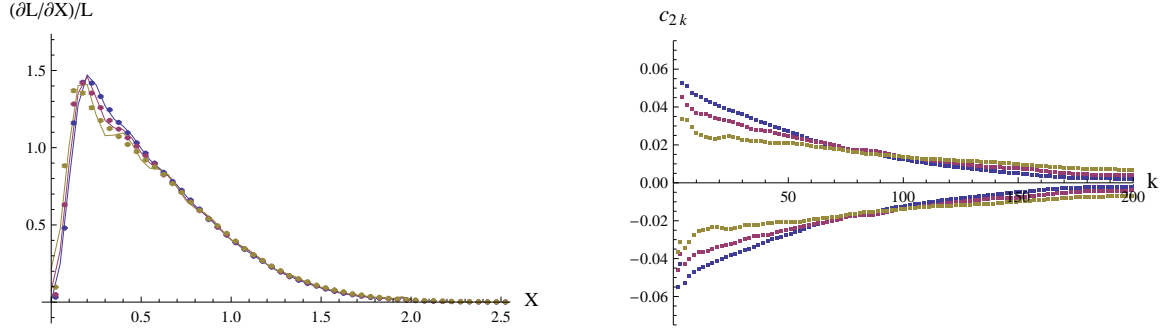


Figure 10. *left:* measured $\partial\mathcal{L}/\partial X/L$ as a function of $X \equiv |\nabla\rho|$ for $\tilde{\gamma} = 0.71, 0.58$ and 0.38 using the set of 25 2D simulations of 1024^2 Gaussian random fields with scale invariant spectra smoothed over 7 pixels. *Right:* value of the fit parameters c_k (see equation (67)). Note that $c_0 = 1$.

parameterize such deviation expanding the true statistics in Hermite series around the stiff approximation

$$\frac{1}{L} \frac{\partial\mathcal{L}}{\partial X} = \sqrt{\frac{2N}{\pi}} \exp\left[-\frac{N}{2}X^2\right] \left(\sum_{k=0}^{\infty} \frac{c_{2k}(\tilde{\gamma})}{\sqrt{(2k)!}} H_{2k}(\sqrt{N}X) \right). \quad (67)$$

This choice of expansion is dictated by the orthogonality of the Hermite polynomials with the weight $\propto \exp[-\sqrt{N}X^2/2]$ on the interval $X \geq 0$. Thus, $c_0 = 1$. If the deviation from the stiff approximation is small, one expects the expansion to be dominated by the $n = 0$ term, while the subsequent terms should quickly fall in a orderly fashion.

To gain understanding on how the coefficients $c_{2k}(\tilde{\gamma})$ behave with $\tilde{\gamma}$, let us consider again the lax situation, opposite to the stiff case, when the third derivatives of the field dominate the length statistics. Our starting point is equation (64) which has the following structure when we consider the differential length with respect to the $|x_1| = X$

$$\frac{\partial\mathcal{L}}{\partial X}^{\text{lax}} \propto X^2 \exp\left[-\frac{3}{2}X^2\right] \int du_1 \left\{ \frac{\exp\left[-\frac{3}{2}\frac{(u_1 - \tilde{\gamma}X)^2}{1 - \tilde{\gamma}^2}\right] + \exp\left[-\frac{3}{2}\frac{(u_1 + \tilde{\gamma}X)^2}{1 - \tilde{\gamma}^2}\right]}{\sqrt{2\pi(1 - \tilde{\gamma}^2)}} \right\} \int d^9 x_{ijk} \psi(x_{ijk}) \bar{P}_1(x_2 = x_3 = 0, x_{ijk}/u_1) \quad (68)$$

where \bar{P}_1 is given by equation (D6) with the dependence on u_1 factored out. The difference with the stiff approximation is large even for $\tilde{\gamma} = 0$ as the gradient's dependence becomes $\propto X^2 \exp[-3/2X^2]$ in place of the stiff scaling $\propto \exp[-3/2X^2]$. Using now this factor as the weight, for $\tilde{\gamma} \neq 0$ we expand the expression in the brackets in generalized Laguerre polynomials. The expansion coefficients are of the form $\tilde{\gamma}^{2k} \exp[-3u_1^2/2] \sum_{m=0}^k d_m \tilde{\gamma}^{2m} H_{2m}(\sqrt{3}u_1)$; denoting the result of the integration of the expansion coefficients and all of the residual factors over the third derivatives by $\Psi_k(\tilde{\gamma})$ we obtain

$$\frac{1}{L} \frac{\partial\mathcal{L}}{\partial X}^{\text{lax}} = 3\sqrt{\frac{6}{\pi}} X^2 \exp\left[-\frac{3}{2}X^2\right] \sum_{k=0}^{\infty} \frac{2^k k!}{(2k+1)!!} \tilde{\gamma}^{2k} L_k^{(1/2)}(3X^2/2) \Psi_k(\tilde{\gamma}), \quad (69)$$

where, again, $\Psi_0(\tilde{\gamma}) = 1$. With the help of the relation between the Laguerre and Hermite polynomials

$$3X^2 k! L_k^{(1/2)}(3/2X^2) = (-1)^k 2^{-k} \left(H_{2k+2}(\sqrt{3}X) + (2k+1)H_{2k}(\sqrt{3}X) \right),$$

we can cast equation (69) in the form of equation (67)

$$\begin{aligned} \frac{1}{L} \frac{\partial\mathcal{L}}{\partial X}^{\text{lax}} &= \sqrt{\frac{6}{\pi}} \exp\left[-\frac{3}{2}X^2\right] \sum_{k=0}^{\infty} \frac{(-1)^k}{(2k+1)!!} \tilde{\gamma}^{2k} \left(H_{2k+2}(\sqrt{3}X) + (2k+1)H_{2k}(\sqrt{3}X) \right) \Psi_k(\tilde{\gamma}), \\ &= \sqrt{\frac{6}{\pi}} \exp\left[-\frac{3}{2}X^2\right] \left[1 + \sum_{k=1}^{\infty} \frac{(-1)^{k-1}}{(2k-1)!!} \left[\tilde{\gamma}^{2k-2} \Psi_{k-1}(\tilde{\gamma}) - \tilde{\gamma}^{2k} \Psi_k(\tilde{\gamma}) \right] H_{2k}(\sqrt{3}X) \right]. \end{aligned} \quad (70)$$

The coefficients $c_{2k}(\tilde{\gamma})$ are

$$c_0 = 1, \quad c_2 = \sqrt{2} (1 - \tilde{\gamma}^2 \Psi_1(\tilde{\gamma})), \quad c_{2k} = \left((-1)^{k-1} \sqrt{(2k)!}/(2k-1)!! \right) \tilde{\gamma}^{2k-2} (\Psi_{k-1}(\tilde{\gamma}) - \tilde{\gamma}^2 \Psi_k(\tilde{\gamma})). \quad (71)$$

In particular, in the limit $\tilde{\gamma} \rightarrow 0$ the first two coefficients remain finite and of equally significant magnitude $c_0 = 1$, $c_2 = \sqrt{2}$, while all the other ones vanish.

Figure 10 and Figure 11 present the measurements of $\partial\mathcal{L}/\partial X/L$ in 2 and 3D respectively, together with the corresponding coefficients given by equation (67). It is found that these coefficients are significantly smaller in two dimensions, a clear indication that the stiff approximation holds better in 2D.

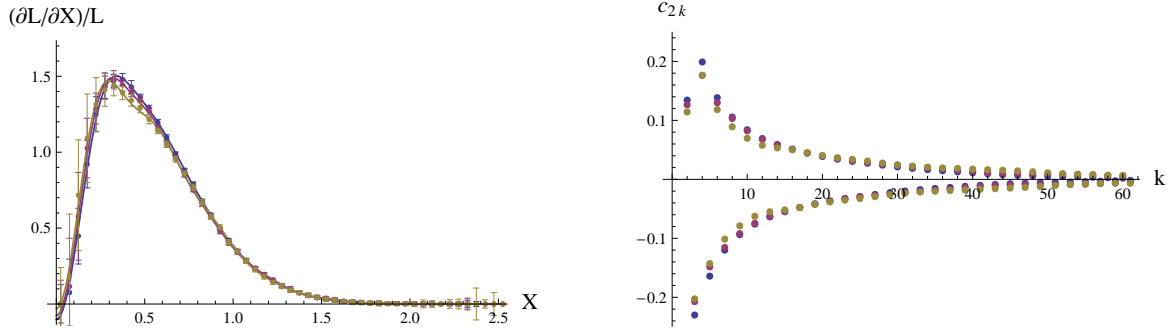


Figure 11. *left:* measured $\partial\mathcal{L}/\partial X/L$ as a function of $X \equiv |\nabla\rho|$ for $\tilde{\gamma} = 0.86, 0.83$ and 0.79 using the set of 3D simulation of 128^3 Gaussian random fields with scale invariant spectra smoothed over 7 pixels. *Right:* value of the fit parameters c_k , Note its faster convergence combined with a larger amplitude relative to the 2D case.

5.2 Statistics of the curvature of the critical lines

The local curvature, κ , at a point on a curve specified by the tangent vector $\mathbf{u} = d\mathbf{r}/dt$ is determined by the acceleration of the tangent vector $\dot{\mathbf{u}} \equiv d\mathbf{u}/dt = \mathbf{u} \cdot (\partial\mathbf{u}/\partial\mathbf{r})$ transverse to the curve direction:

$$\kappa = \frac{|\mathbf{u} \times \dot{\mathbf{u}}|}{|\mathbf{u}|^3} = \frac{|\mathbf{u} \times ((\nabla\mathbf{u}) \cdot \mathbf{u})|}{|\mathbf{u}|^3}. \quad (72)$$

Importantly, the curvature does not depend on parameterization t , nor on normalization of the tangent vector \mathbf{u} . In the local theory, the tangent vector to a critical line is orthogonal to $\nabla s^i(x_k, x_{kl})$ and can be taken to be

$$\mathbf{u} = \boldsymbol{\epsilon} \cdot \nabla s \quad (2D), \quad \mathbf{u} = \nabla s^i \cdot \boldsymbol{\epsilon} \cdot \nabla s^j = \nabla s^i \times \nabla s^j \quad (3D); \quad (73)$$

so the curvature κ is the random quantity which involves the derivatives of the field up to fourth order,

$$(2D) \quad \kappa = |\nabla s \cdot (\nabla\nabla s) \cdot \nabla s| / |\nabla s|^3, \quad (74)$$

$$(3D) \quad \kappa = \left| \left(\nabla s^i \times \nabla s^j \right) \times \left[\left(\nabla s^i \times \nabla s^j \right) \cdot \nabla \left(\nabla s^i \times \nabla s^j \right) \right] \right| / \left| \nabla s^i \times \nabla s^j \right|^3. \quad (75)$$

The curvature of the critical lines fundamentally reflects the derivatives of the field higher than the second. If they are neglected, the curvature is identically zero. Explicitly, the contributions that do not involve higher derivatives, in 2D

$$(2D) \quad (\mathbf{u} \times \dot{\mathbf{u}})^2 = 4x_1^2 x_2^2 \lambda_1^4 (\lambda_1 - \lambda_2)^6 \lambda_2^4 + \dots, \quad (76)$$

$$(3D) \quad (\mathbf{u} \times \dot{\mathbf{u}})^2 = (x_2^2 \lambda_3^2 + x_3^2 \lambda_2^2) (\lambda_1 - \lambda_2)^4 (\lambda_1 - \lambda_3)^4 \lambda_1^2 (3x_1^2 \lambda_2^2 \lambda_3^2 + (x_2^2 \lambda_3^2 + x_3^2 \lambda_2^2) \lambda_1^2)^2 + \dots, \quad (77)$$

vanish when the correspondent critical line conditions $x_2 = 0$ or $x_2 = x_3 = 0$ are applied¹¹.

The integrated curvature over the length of the line, $\mathcal{C} = \int \kappa dL$ is a useful dimensionless characteristics of the overall extend a line is curved. We have seen that the critical line length in volume dV is $dL \propto |\nabla s| \delta_D(s) dV$ and $dL \propto |\nabla s^i \times \nabla s^j| \delta_D(s^i) \delta_D(s^j) dV$ in 2D and 3D respectively. Averaging over statistical distribution in regions above threshold η we obtain the mean density of the integrated critical line curvature $\mathcal{C} = \langle d\mathcal{C}/dV \rangle$

$$(2D) \quad \mathcal{C}(\eta_{>}) = \frac{1}{R_* \bar{R}} \int_{\eta_{>}} dx d^2 x_k d^3 x_{kl} d^4 x_{klm} d^5 x_{klmn} \kappa(x_k, x_{kl}, \dots) |\nabla s| \delta_D(s) P(x, x_k, x_{kl}, \dots), \quad (78)$$

$$(3D) \quad \mathcal{C}(\eta_{>}) = \frac{1}{R_*^2 \bar{R}} \int_{\eta_{>}} dx d^3 x_k d^6 x_{kl} d^{10} x_{klm} d^{15} x_{klmn} \kappa(x_k, x_{kl}, \dots) \left| \nabla s^i \times \nabla s^j \right| \delta_D(s^i) \delta_D(s^j) P(x, x_k, x_{kl}, \dots), \quad (79)$$

where the integration is carried over all the derivatives up to the fourth order. The required joint probability function is given in equations (D19) and (D21).

Let us consider 2D case and estimate the curvature by using stiff approximation for the tangent vector u while following its local variation which involve higher derivatives of the underlying field. In the Hessian eigenframe, assuming the skeleton lies along 1, if \mathbf{u} is approximated by its stiff counterpart we have:

$$\left(\frac{|\mathbf{u} \times \dot{\mathbf{u}}|}{|\mathbf{u}|^2} \right)^{\text{stiff}} = |x_1| |(\lambda_1 + \lambda_2) x_{112}|, \quad (80)$$

¹¹ Note that by construction, the torsion: $\tau = |\mathbf{u} \cdot (\dot{\mathbf{u}} \times \ddot{\mathbf{u}})| / |\mathbf{u} \times \dot{\mathbf{u}}|^2$ contains only the terms proportional to at least the third derivatives of the field.

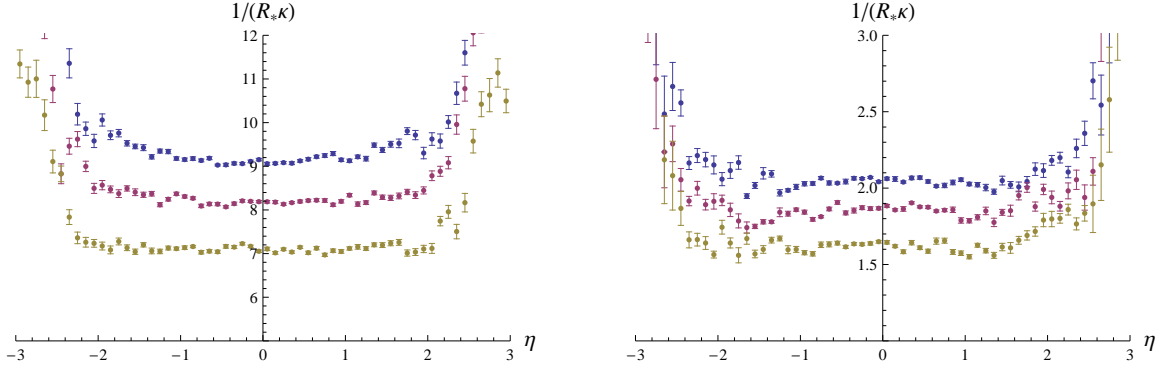


Figure 12. $1/(R_*\langle\kappa\rangle)$, the mean curvature radius in units of R^* as a function of η measured in simulation of 2D (left) and 3D (right) Gaussian random fields with scale invariant power-law spectra. The top curves correspond to spectra with more power at small scales and higher γ and $\tilde{\gamma}$ spectral parameters.

so that (taking into account the measure in the eigenframe and the δ_D function of S in x_2):

$$\begin{aligned} \frac{\partial \mathcal{C}^{\text{stiff}}}{\partial \eta} &= \pi \int d\lambda_1 d\lambda_2 d^4 x_{ijk} |(\lambda_1 + \lambda_2)x_{112}| P_0(\eta, x_{kl}) P_1(x_{ijk}) \\ &= \frac{\sqrt{2 - \tilde{\gamma}^2}}{4\pi R_* \tilde{R}} \left(\sqrt{2(1 - \gamma^2)} \exp\left[-\frac{\gamma^2 \eta^2}{2(1 - \gamma^2)}\right] + \sqrt{\pi} \text{Erf}\left[\frac{\gamma \eta}{\sqrt{2(1 - \gamma^2)}}\right] \gamma \eta \right) \frac{1}{\sqrt{2\pi}} \exp\left[-\frac{\eta^2}{2}\right], \end{aligned} \quad (81)$$

the last evaluation being done for the primary critical lines.

We have measured the mean curvature of the skeleton lines at the threshold η ,

$$\langle\kappa\rangle \equiv \frac{\partial \mathcal{C} / \partial \eta}{\partial \mathcal{L} / \partial \eta}, \quad (82)$$

in simulations of the Gaussian random fields of different spectra, using the global skeleton techniques. Figure (12) displays the 2D (left panel) and 3D (right panel) results in terms of the curvature radius, $R_{\text{curv}} = 1/\langle\kappa\rangle$. The measurements show that for the spectra we consider, the averaged curvature is insensitive to the density threshold for low-to-moderate threshold values showing a plateau in the interval $-2 < \eta < 2$. This indicates that in this regime the curvature of the skeleton does not depend on γ , but rather on $\tilde{\gamma}$ and perhaps $\hat{\gamma}$. It follows that in 3D the critical lines are relatively more wiggly than in 2D. If we use the lower value of R_{curv}^{3D} as a guidance, it seems the stiff approximation is less accurate in 3D than in 2D, as could be expected. The stiff estimate (81) gives the threshold-averaged mean density of the integrated curvature $\mathcal{C}^{\text{stiff}}$ and, using equation (37), the mean curvature radius, $R_{\text{curv}}^{\text{stiff}}$, as

$$\mathcal{C}^{\text{stiff}} = \frac{\sqrt{1 - \tilde{\gamma}^2/2}}{2\pi R_* \tilde{R}}, \quad R_{\text{curv}}^{\text{stiff}} \equiv \frac{L}{\mathcal{C}} = \frac{\sqrt{2} + \pi/2}{\sqrt{1 - \tilde{\gamma}^2/2}} \tilde{R} \approx 2.985 \frac{\tilde{\gamma}}{\sqrt{1 - \tilde{\gamma}^2/2}} R_*. \quad (83)$$

This result captures the qualitative dependence on $\tilde{\gamma}$ observed in simulations, but is a factor of three smaller in the magnitude of the curvature radius. This shows that the global skeleton, used in the numerical measurement, is notably straighter than the local critical lines, although the dependence of curvature on the spectral parameters seems similar.

Note in closing that in 2D, (resp. 3D) the knowledge of the differential length, curvature (resp. length, curvature and torsion) corresponds to an exhaustive global statistical description of the critical lines.

5.3 Singular points of critical lines

Let us now ask ourselves the following question: are there any special points along the skeleton? The obvious ones are the extrema of the field itself where critical lines intersect. Beyond this, one can anticipate two other types of singular points. The first type corresponds to points where the curvature transverse to the direction of the critical line vanishes along at least one axis: typically, in 2D, they mark regions where a crest becomes a trough, or vanish into a plateau. The second type correspond to points where the critical lines would split, even though the field does not go through an extremum: a bifurcation of the lines occurs along the slope; the occasional skier or mountaineer will be familiar with a crest line splitting in two, even though the gradient of the field has not vanished. From the point of view of the theory of random fields, the frequency of such points is an interesting venue: indeed we expect that steep power spectrum present relatively more bifurcation points as \tilde{R} , the distance between inflection points (see Sec. 2.2), becomes much shorter than R_* , the distance between extrema. In an astrophysical context, the statistical properties of the first type of points, and in particular their clustering properties are of interest for understanding the geometry of galactic infall, which in turn is believed to play an important role in defining the morphological properties of galaxies. The multiplicity of the maxima (*i.e.* the number of connected skeleton segments) is also of interest in the context of galaxy formation and feedback. In more abstract spaces, such as position-time, identifying bifurcations is important to pin down merging events (see e.g. Hanami (2001) and Appendix A).

5.3.1 Defining the skeleton singular points

Formally a singular condition along the skeleton occurs when at some point the determination of the critical line direction fails. It means that at this point the matrix $\nabla_k S^i$ of equation (2) has more than one distinct *right* null-vector, or, equivalently, all M^k defined by equation (A7) are zero. The only case when it happens exactly is at the extremal points of the field $\nabla\rho = 0$. There are no other formal singularities on the local critical lines, since when $\nabla\rho \neq 0$, the requirement $M^k = 0$ sets N relations between the field gradient, second and third derivatives which have vanishing probability to be simultaneously satisfied along a line in a random field.

The failure of the formal definition to identify all the physically interesting situations primarily reflects the inadequacy of the local skeleton construction, which only utilizes locally quadratic approximation to the field, to map the field near the singular points.¹² Figure 13 gives a 2D example. In 2D, the critical lines are zero levels of the scalar S -function, while $\nabla S = 0$ at the extrema of S field. In Figure 13 the region where a ridge splits into two is shown. One expect two critical lines cross there, with three branches following the ridges, and one following the through between two of the split branches. Instead, the locally defined critical lines are not allowed to join at the bifurcation point since the formal condition $\nabla S = 0$ is satisfied just *off* $S = 0$ contour, rather they artificially reconnect near the bifurcation point into two non-intersecting segments.

We conjecture that the critical lines experience a qualitative change in behaviour in the vicinity of the points where either the Hessian eigenvalue of the orthogonal to the gradient direction vanish, or becomes equal to the one along the gradient. Namely, if, for definiteness, $\nabla\rho$ is taken to be along the first eigen-direction, $\lambda_2 = 0$, or $\lambda_2 = \lambda_1$. We call the first case the “sloping plateau” as it designates the entering of a flat region, and the second, tentatively, the “bifurcation” as it designates the places of possible reconnection of critical lines. In particular, at the $\lambda_2 = \lambda_1$ points most of the transitions from primary to secondary behaviour take place. Remarkably, these special points on the critical lines are recovered by the formal singular condition $|M^k| = 0$ if $\nabla_k S^i$ is evaluated in the stiff approximation. As given in equation (A12), along the ND critical line defined by $x_2 = \dots = x_N = 0$, $|M^{\text{stiff}}| = x_1^{N-1} \prod_{i>1} \lambda_i (\lambda_1 - \lambda_i) = 0$ gives rise to three classes of situations: (i) $x_1 = 0$ corresponding to extremal points; (ii) one of $\lambda_i = 0$ corresponding to slopping flattened tubes; and (iii) one of $\lambda_i = \lambda_1$, corresponding to an isotropic bifurcation.

Since it is beyond the scope of this paper to develop the full theory of these special points, we will focus here on their number density for isotropic 2D Gaussian random fields, leaving more detailed investigation to future work.

5.3.2 Number density of the singular points of the 2D critical lines

In 2D, the skeleton’s singular points correspond to points where $S_k \equiv \nabla_k S = \mathbf{0}$. The number density, $n_B(\eta)$ of singular points below the threshold η is equal to

$$n_B(\eta) = \int_{\eta>x} dx d^2 x_k d^3 x_{kl} d^4 x_{klm} d^5 x_{klmn} P(x, x_k, x_{kl}, \dots) |\det(\nabla_k \nabla_l S)| \delta_D(s_1) \delta_D(s_2). \quad (84)$$

The simplest case of the skeleton singular points $\nabla S = \mathbf{0}$ are, according to equation (8), the extrema of the field itself, $x_1 = x_2 = 0$. Indeed when both x_1 and x_2 vanish

$$|\det(\nabla_k \nabla_l S)| \delta_D(s_1) \delta_D(s_2) = |x_{kl}| \delta_D(x_1) \delta_D(x_2), \quad (85)$$

which is exactly the integrand involved in the number density of *extrema* of the field. The extrema number densities, for reference, are given in 2D by (Longuet-Higgins 1957)

$$\frac{\partial n_{\text{saddle}}}{\partial \eta} = \frac{1}{R_*^2} \frac{1}{4\sqrt{3}} \left[\frac{1}{\sqrt{2\pi} \sqrt{1-2\gamma^2/3}} \exp\left(-\frac{\eta^2}{2(1-2\gamma^2/3)}\right) \right], \quad (86)$$

$$\frac{\partial n_{\text{min+max}}}{\partial \eta} = \frac{\partial n_{\text{saddle}}}{\partial \eta} + \frac{1}{4R_*^2} \gamma^2 (-1 + \eta^2) \frac{1}{\sqrt{2\pi}} \exp\left(-\frac{\eta^2}{2}\right). \quad (87)$$

The singularity of the extrema from the points of view of the critical line theory is manifest in the fact that at extrema several critical lines intersect.

The gradient of S , evaluated in the stiff approximation, in the Hessian eigenframe has the components

$$s_1^{\text{stiff}} = x_2 \lambda_1 (\lambda_1 - \lambda_2), \quad \text{and} \quad s_2^{\text{stiff}} = x_1 \lambda_2 (\lambda_1 - \lambda_2). \quad (88)$$

and involves only second derivatives of the field. Remarkably, within this approximation, there are new singular points that lie *on* the (local) critical lines. The reason is that among two conditions needed for ∇S to vanish, one is already automatically satisfied by being on a critical line.

To be specific, let us consider the critical line that corresponds to the $x_2 = 0$ condition in the Hessian eigenframe. Then s_1^{stiff} vanishes everywhere along this line. The requirement $s_2^{\text{stiff}} = 0$ has a solution at the extremal points, $x_1 = 0$, but also in two other cases, namely $\lambda_2 = 0$ or $\lambda_2 = \lambda_1$, that we conjectured to be of interest.

¹² Similarly, the bifurcation points for the global fully-connected skeleton (Sousbie et al. 2008) also formally merge with critical points in the strict sense due to sharp topological theorems (Jost 2008). However they appear if the skeleton is viewed with a finite resolution.

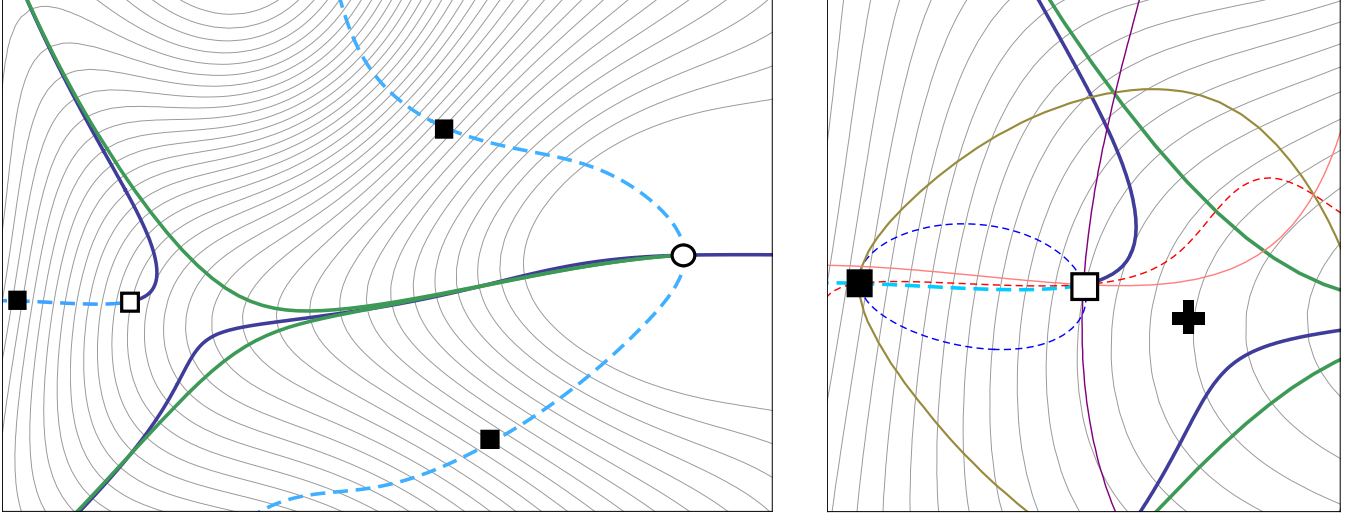


Figure 13. *Left:* the three types of singular point on the critical lines (in solid blue: primary; dashed: secondary; green: gradient lines of the global skeleton): an extremum (open circle), a “bifurcation” (white square), and “sloping plateaux” (black squares). The thin lines are the isocontours of the field. *Right:* Detailed view of the bifurcation region: The pink and purple lines mark the conditions $x_{11} = x_{22}$ and $x_{12} = 0$, which when intersect give the point where $\lambda_1 = \lambda_2$. This point is a singular point of the critical line (white square). The gold line is the condition $\lambda_2 = 0$ that marks the “sloping plateau” on the critical lines. The red and blue dashed lines are zero isocontours of two components of ∇S^{stiff} . The $\nabla S^{\text{stiff}} = 0$ criterium pin-points exactly all types of the singular points on the critical lines. The black cross marks the position of the point $\nabla S = 0$.

The first situation, *the sloping plateau* with a flat transverse gradient, only occurs on secondary critical lines since it implies $\lambda_1 > 0$, and corresponds to

$$\left| \det \left(\nabla_{(k} s_l^{\text{stiff}} \right) \right| \delta_{\text{D}}(s_1) \delta_{\text{D}}(s_2) = \left| \frac{x_1 x_{112} x_{222}}{(\lambda_1 - \lambda_2)} \right| \delta_{\text{D}}(\lambda_2) \delta_{\text{D}}(x_2), \quad (89)$$

hence

$$\begin{aligned} \frac{\partial n_{\text{B}}^{\text{F}}}{\partial \eta} &= \frac{1}{\tilde{R}^2} \int d\lambda_1 P_0(\eta, \lambda_1, \lambda_2 = 0) \times \int dx_1 d^4 x_{klm} P_1(x_1, x_2 = 0, x_{klm}) |x_1 x_{112} x_{222}| + (1 \rightarrow 2, \eta \rightarrow -\eta), \\ &= \frac{1}{\sqrt{3}\pi^2 \tilde{R}^2} \left[\frac{1}{\sqrt{2\pi} \sqrt{1 - 2\tilde{\gamma}^2/3}} \exp\left(-\frac{\eta^2}{2(1 - 2\tilde{\gamma}^2/3)}\right) \right] \left[\sqrt{1 - \tilde{\gamma}^2} + \frac{1}{4}(2 - 3\tilde{\gamma}^2) \text{atan}\left(\frac{2 - 3\tilde{\gamma}^2}{4\sqrt{1 - \tilde{\gamma}^2}}\right) \right], \\ &\equiv \frac{4}{\tilde{\gamma}^2 \pi^2} \mathcal{G}_B^{\text{F}}(\tilde{\gamma}) \frac{\partial n_{\text{saddle}}}{\partial \eta}. \end{aligned} \quad (90)$$

The second situation (isotropic Hessian) corresponds to

$$\left| \det \left(\nabla_{(k} s_l^{\text{stiff}} \right) \right| \delta_{\text{D}}(s_1) \delta_{\text{D}}(s_2) = \frac{1}{4} \left| \frac{x_1 (u_2^2 - 16(w_1^2 + w_2^2))}{(\lambda_1 - \lambda_2)} \right| \delta_{\text{D}}(\lambda_1 - \lambda_2) \delta_{\text{D}}(x_2),$$

therefore

$$\begin{aligned} \frac{\partial n_{\text{B}}^{\text{I}}}{\partial \eta} &= \frac{1}{\tilde{R}^2} \int d\lambda_1 P_0(\eta, \lambda_1, \lambda_2 = \lambda_1) \times \int dx_1 d^4 x_{klm} P_1(x_1, x_2 = 0, x_{klm}) |x_1 (u_2^2/4 - 4(w_1^2 + w_2^2))| + (1 \rightarrow 2, \eta \rightarrow -\eta), \\ &= \frac{1}{\pi \tilde{R}^2} \left[\frac{1}{\sqrt{2\pi}} \exp\left(-\frac{\eta^2}{2}\right) \right] \left[\frac{2}{\sqrt{2 - \tilde{\gamma}^2}} - \frac{1}{2}(1 + \tilde{\gamma}^2) \right] \equiv \frac{1}{\tilde{\gamma}^2 \pi R_*^2} \mathcal{G}_B^{\text{I}}(\tilde{\gamma}) P(\eta). \end{aligned} \quad (91)$$

Both $\mathcal{G}_B^{\text{F}}(\tilde{\gamma})$ and $\mathcal{G}_B^{\text{I}}(\tilde{\gamma})$ are weak functions of $\tilde{\gamma}$ of order unity. The main $\tilde{\gamma}$ dependence $\propto \tilde{\gamma}^{-2}$ reflects \tilde{R} as the fundamental scale for the singular points.

We note that the number density of the “sloping plateaux” is proportional to the density of the saddle points, hence this type of singular points is predominantly concentrated near mean field values (small η). In contrast, the number density of “bifurcation” points is proportional just to the PDF of the field and, hence, the bifurcation points are as frequent in the regions of high field values as in the low ones. This may provide explanation for the observed insensitivity of the curvature of the skeleton to the threshold, if we conjecture that most of the curvature accumulates near the “bifurcation” points.

2D		3D	
Skeleton	$4.21R_*$	Skeleton:	$(4.65R_*)^2$
Anti-skeleton	$4.21R_*$	Anti-skeleton:	$(4.65R_*)^2$
		Inter-skeleton:	$(3.38R_*)^2$
All primary	$2.11R_*$	All primary	$(2.36R_*)^2$
All secondary	$5.54R_*$	All secondary	$(3.02R_*)^2$
Total	$1.55R_*$	Total	$(1.86R_*)^2$

Table 3. Inverse average integrated flux (the characteristic area (3D) or length (2D) per critical line) of the critical lines of different types.

6 CONCLUSION & PERSPECTIVES

The filamentary structure is a dramatic feature of the observed or simulated Cosmic Web. This paper investigated how the set of critical lines of a given field corresponds to an intermediate representation of the field, which is more extended than the knowledge of the critical points, but nevertheless much more compact than the field itself. It introduced the stiff approximation, which states that the tangent vector to the critical lines only involves up to the second derivative of the fields. Within its framework it has been demonstrated that, for stationary Gaussian random fields, ergodicity allows one to recast the description of the ND critical lines into a point process, which only involve the first spectral parameter, γ , when considering the differential length as a function of the contrast, and the second spectral parameter, $\tilde{\gamma}$, when considering it as a function of the modulus of the gradient. The former probability distribution was shown to involve the average flux of the Gaussian curvature of the 1D sections. In turn, these averages can be carried out analytically almost to the last integral in 2D and 3D, and provide simple asymptotics at large and small contrast. The detailed contribution of all types of critical lines as a function of thresholding was described. The main results of this investigation corresponds to equations (27) and (28) for the differential length of the skeleton and the total set of critical lines in 2D and equations (48) and (51) in 3D. Their generalization to N dimensions is given by equation (A18) in Appendix A. Table 3 summarizes the average integrated fluxes (i.e length per unit volume) of the critical lines. For instance in 3D one expect on average one skeleton line crossing a random $\approx (5R_*)^2$ surface element.

These findings were illustrated on scale free power spectra with spectral parameters which are relevant to cosmology¹³. The prediction of the stiff approximation was checked against measurements for global skeletons (Sousbie et al. 2008) on realizations of these fields in two and three dimensions and was found to be in good qualitative agreement. The differential curvature of the corresponding lines was also measured (section 5.2) and the corresponding radii were found to be $\approx 8R_*$ and $\approx 2.5R_*$ near $\eta = 0$ in two and three dimensions respectively. Hence an access to both the curvature and the length of the skeleton provides the means of constraining two shape parameters, γ and $\tilde{\gamma}$. The stiff approximation is also implemented to compute the differential curvature in 2D. Finally (section 5.3), the stiff theory of the singular points of the critical lines was laid out in general, identifying generically three types of points: critical points of the underlying field, bifurcation points and stopping plateaux. Again, the stiff approximation provide means of computing the number density of these points. Appendix D derived the general joint probability of the field and its successive derivative in arbitrary dimensions, which come into play when computing these higher order statistics.

Clearly the formalism developed in this paper will be useful in the context of the upcoming surveys such as the LSST, or the SDSS-3 BAO surveys since it yields access to the shape of the power-spectrum without artifacts related to varying light to mass ratio. For instance, Sousbie et al. (2008) first applied the corresponding theory to the SDSS-DR4 catalogue in order to constraint the global dark matter content of the universe, since the cosmological parameters are directly a function of the spectral parameter, γ . Its application to CMB related full sky data, such as WMAP or Planck should provide insight into, e.g. the level of non-Gaussianity in these maps (see SPCNP for a discussion). Similarly, upcoming large scale weak lensing surveys could be analyzed in terms of these tools (Pichon et al. 2009).

A natural extension of the theoretical component of this work would be to investigate the properties of the bifurcation points in anisotropic settings and extend beyond the stiff approximation the preliminary results of Section 5.3. This will be the topic of a forthcoming paper. Another natural venue would be to also investigate the statistical properties of, e.g. the peak patch walls (surface, curvature) defined as $x_3 = 0$ in the eigenframe of the Hessian. Eventually, a global theory of the critical manifolds beyond the local approximation should also be developed to provide a framework to study the connectivity of the critical lines.

ACKNOWLEDGMENTS

We thank D. Aubert and K. Benabed for comments and D. Munro for freely distributing his Yorick programming language and opengl interface (available at <http://yorick.sourceforge.net/>). DP thanks the CNRS (France) for support through a

¹³ in other fields, the stiff approximation might be less well motivated (see Section 4.4), but the calculations hold.

“poste rouge” visiting position during Summer 2007 when this investigation was originated. CP, TS, SP and CG also thank the hospitality of the University of Alberta, and the “Programme National de Cosmologie” for funding. Finally, CP and DP thank the Canadian Institute for Theoretical Astrophysics for hosting the work involved in finalizing this paper. This investigation carried within the framework of the Horizon project, www.projet-horizon.fr.

REFERENCES

- Adler R. J., 1981, The Geometry of Random Fields. The Geometry of Random Fields, Chichester: Wiley, 1981
- Aragón-Calvo M. A., Jones B. J. T., van de Weygaert R., van der Hulst J. M., 2007, *aap*, 474, 315
- Arnol’d V. I., Zel’dovich Y. B., Shandarin S. F., 1981, *Usp. Mat. Nauk*, Tom 36, p. 244 - 245, 36, 244
- Bardeen J. M., Bond J. R., Kaiser N., Szalay A. S., 1986, *ApJ*, 304, 15
- Bond J. R., Kofman L., Pogosyan D., 1996, *Nature*, 380, 603
- Bond J. R., Myers S. T., 1996a, *ApJ Sup.*, 103, 1
- Bond J. R., Myers S. T., 1996b, *ApJ Sup.*, 103, 63
- Cardoso J.-F., 2009, In preparation
- Colombi S., Pogosyan D., Souradeep T., 2000, *Physical Review Letters*, 85, 5515
- Doroshkevich A. G., 1970, *Astrophysics*, 6, 320
- Hanami H., 2001, *MNRAS*, 327, 721
- Jost J., 2008, *Riemannian Geometry and Geometric Analysis*, Fifth Edition. Berlin ; New York : Springer, c2008.
- Kaiser N., 1984, *ApJ Let.*, 284, L9
- Longuet-Higgins M. S., 1957, *Royal Society of London Philosophical Transactions Series A*, 249, 321
- Novikov D., Colombi S., Doré O., 2006, *MNRAS*, 366, 1201
- Pichon C., Bernardeau F., 1999, *Astronomy and Astrophysics*, 343, 663
- Pichon C., Thibaut E., Prunet S., Benabed K., Sousbie T., Teyssier R., 2009, *MNRAS*, 0, 0
- Platen E., van de Weygaert R., Jones B. J. T., 2007, *MNRAS*, 380, 551
- Pogosyan D., Bond J. R., Kofman L., Wadsley J., 1998, in Colombi S., Mellier Y., Raban B., eds, *Wide Field Surveys in Cosmology Cosmic Web: Origin and Observables*. pp 61–66
- Regos E., Szalay A. S., 1995, *MNRAS*, 272, 447
- Scannapieco E., Pichon C., Aracil B., Petitjean P., Thacker R. J., Pogosyan D., Bergeron J., Couchman H. M. P., 2006, *MNRAS*, 365, 615
- Schmalzing J., Buchert T., Melott A. L., Sahni V., Sathyaprakash B. S., Shandarin S. F., 1999, *ApJ*, 526, 568
- Sousbie T., Colombi S., Pichon C., 2008, *MNRAS*
- Sousbie T., Pichon C., Colombi S., Novikov D., Pogosyan D., 2008, *MNRAS*, 383, 1655
- Sousbie T., Pichon C., Courtois H., Colombi S., Novikov D., 2008, *ApJ Let.*, 672, L1

APPENDIX A: THE STIFF SKELETONS OF ND FIELDS

The emphasis in this paper is on developing the analytical theory of the critical lines of a given GRF in two and three dimensions. Yet the critical lines in higher dimensions are of interest in more abstract spaces such as space-time or space-smoothing etc. . In 3+1 Dimensions, corresponding to 3D space+time, the 4D critical lines are the dynamical tracks of critical points in 3D. An alternative view is to think of the 4D skeleton as event lines of over densities, while the critical points correspond to the position and time of merging events. In fact Hanami (2001) explored sloping saddles (i.e. points in position-smoothing space corresponding degenerate saddle points) as a mean of identifying merging events, and argued that the ridges (the path of the maxima in position-smoothing space as a function of smoothing) form a 4D skeleton. Clearly these higher dimensional spaces would typically not be strictly isotropic, stationary nor Gaussian. As a first step, let us nonetheless investigate these N dimensional lines.

A1 Critical Lines in ND

The local critical lines in N dimensions are defined as the points where the condition

$$\mathcal{H} \cdot \nabla \rho = \lambda_i \nabla \rho, \quad (\text{A1})$$

is satisfied. This can be expressed as the condition of the vanishing of the $N - 2$ antisymmetric tensor

$$\mathbf{S} = S^{i_1, i_2, \dots, i_{N-2}} \equiv \sum_{klm} \nabla_k \rho H^k_l \epsilon^{i_1, \dots, i_{N-2}, l, m} \nabla_m \rho = 0 \quad (\text{A2})$$

as defined in equation (1). In spaces of dimension $N > 4$ it is more compact to consider the Hodge-dual rank 2 tensor

$$(*\mathbf{S}) = (*S)^{ij} = \frac{1}{(N-2)!} \sum_{i_1, \dots, i_{N-2}} S^{i_1, i_2, \dots, i_{N-2}} \epsilon_{i_1, \dots, i_{N-2}, i, j} = 0 \quad (\text{A3})$$

Local direction of the filament corresponds to the *right* null-vector δr^k of the $N - 2 + 1$ -rank tensor of the derivatives of \mathbf{S}

$$\sum_k \left(\nabla_k S^{i_1, i_2, \dots, i_{N-2}} \right) \delta r^k = 0 \quad . \quad (\text{A4})$$

A non-trivial solution of this set of C_N^2 homogeneous equations generally exists, since the existence of the *left* null-vector $\sum_{i_1} \nabla_{i_1} \rho \left(\nabla_k S^{i_1, i_2, \dots, i_{N-2}} \right) = 0$ imposes C_{N-1}^2 linear relations leaving exactly $C_N^2 - C_{N-1}^2 = N - 1$ independent equations to define a line.

The notion of *primary* skeleton lines is automatically generalized for N D as the subset of critical lines obeying

$$\mathcal{H} \cdot \nabla \rho = \lambda_1 \nabla \rho, \quad \text{and} \quad \lambda_1 + \lambda_2 \leq 0, \quad (\text{A5})$$

where λ_1 is the largest and λ_2 is the second largest of the sorted eigenvalues.

Let us derive the general expression for the statistical average of the flux of the lines arbitrarily defined over the properties of the ND random field by $N - 1$ equations $S^i = 0$, $i = 1 \dots N - 1$, where $S^i(x, x_k, x_{kl}, \dots)$ are functions of the field and its derivatives. We can shortcut the procedure of flux evaluation by marking each line with one intersection point with a fiducial surface Σ , orthogonal to it, and finding the $N-1$ number density of the intersection points on the surface $\Sigma = 0$. The average number density of the points defined as the intersection of n non degenerate hypersurfaces $\sigma^1, \dots, \sigma^N$ is given by

$$n = \int dx d^N x_k \dots P(x, x_k, \dots) \delta_D(\sigma^1) \dots \delta_D(\sigma^n) |\det(\nabla \sigma^1, \dots, \nabla \sigma^n)|. \quad (\text{A6})$$

Let us choose $S^1 \dots S^{N-1}$ as $\sigma^2 \dots \sigma^n$ and Σ to be σ^N . Expanding the determinant $|\det(\nabla S^1, \dots, \nabla S^{N-1}, \nabla \Sigma)|$ along its last row we obtain

$$n = \int dx d^N x_k \dots P(x, x_k, \dots) \delta_D(S^1) \dots \delta_D(S^{N-1}) \delta_D(\Sigma) \left| \sum_k M^k \nabla_k \Sigma \right|, \quad (\text{A7})$$

where

$$M^k = (-1)^{k+1} \det \left(\nabla_l S^i \right)_{\substack{i=1, \dots, N-1 \\ l=1, \dots, k-1, k+1, \dots, N}} = \sum_{l_1, \dots, l_{N-1}} \epsilon^{k, l_1, \dots, l_{N-1}} \nabla_{l_1} S^1 \dots \nabla_{l_{N-1}} S^{N-1} \quad (\text{A8})$$

are the corresponding minors. By design the $\Sigma = 0$ surface is to be orthogonal to the line and therefore its normal $\nabla \Sigma$ and the “vector” $\mathbf{M} \equiv (M^k)$ are parallel,

$$\left| \sum_k M^k \nabla_k \Sigma \right| = |\mathbf{M}| |\nabla \Sigma| \quad .$$

Without loss of generality, we can consider the intersection point to be at $\mathbf{r} = 0$ and take $\Sigma = \mathbf{e}_\Sigma \cdot \mathbf{r}$ where \mathbf{e}_Σ is the unit vector in the local direction of the filament, hence $|\nabla \Sigma| = 1$. The average $(N-1)$ D number density of intersection points on Σ surface that gives us the average flux \mathcal{L} is obtained by integrating the volume number density over the coordinate along \mathbf{e}_Σ , $z = \mathbf{e}_\Sigma \cdot \mathbf{r}$, with $\delta_D(\Sigma)$ in equation (A7) properly counting exactly one intersection per line

$$\mathcal{L} \equiv \int n d(\mathbf{e}_\Sigma \cdot \mathbf{r}) = \int dx d^N x_k \dots P(x, x_k, \dots) \delta_D(S^1) \dots \delta_D(S^{N-1}) |\mathbf{M}| \quad . \quad (\text{A9})$$

To apply this general formula to the critical lines one must choose an arbitrary subset of $N - 1$ linearly independent $\nabla S^{i_1, i_2, \dots, i_{N-2}}$ from the set of all C_N^2 of them.

Note that one can also think of \mathcal{L} as the average length of lines per unit volume, which is the interpretation we focus on in the main text.

A2 Stiff critical lines in ND

In the theory of ND critical lines, the $N-1$ independent functions S^i that define the critical condition (A2) acquire the following simple form in the eigenframe of the Hessian of the field

$$s^i = x_a x_i (\lambda_a - \lambda_i) = 0, \quad i \neq a \quad . \quad (\text{A10})$$

Here a is the index of the Hessian eigenvector that the gradient is aligned with, as is obvious from the solution $x_i = 0$, $i \neq a$.

In the stiff approximation, the gradients $s^i_k \equiv \nabla s^i$ have just two non-zero components, $s^i_a = x_i \lambda_a (\lambda_a - \lambda_i)$ (which vanishes on the critical line) and $s^i_i = x_a \lambda_i (\lambda_a - \lambda_i)$. The vector that determines the direction of the critical line becomes

$$M^k = x_a^{N-2} x_k \prod_{i \neq k} \lambda_i \prod_{i \neq a} (\lambda_a - \lambda_i) \quad . \quad (\text{A11})$$

On the critical line, it has just one non-vanishing component

$$M^a = x_a^{N-1} \prod_{i \neq a} \lambda_i (\lambda_a - \lambda_i) = |\mathbf{M}|, \quad (\text{A12})$$

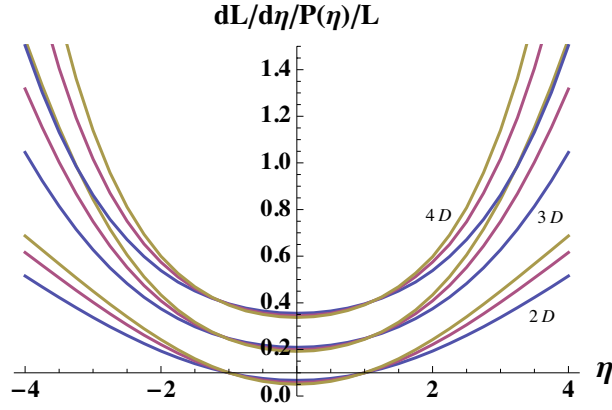


Figure A1. $\partial\mathcal{L}/\partial\eta/P(\eta)/L$ in 2D, 3D and 4D as labeled for the spectral parameter values $\gamma = 0.57, 0.65, 0.70$ (from bottom to top). These quantities are derived here by direct numerical integration of equation (A18). The different bundles corresponding to different dimensions have been shifted down (by 0.3 for 2D and 0.15 for 3D) for clarity. Note the change in the power of the asymptotic curves.

which shows that in the stiff approximation we equate the direction of the line with the gradient of the field. Substituting this expression into equation (A9) and integrating over $\delta_{\text{D}}(s^i) = \delta_{\text{D}}(x_i)/(x_a(\lambda_a - \lambda_i))$ we obtain a simple expression for the flux of the critical lines in the stiff approximation

$$\mathcal{L} = \int dx dx_{kl} P(x, 0, x_{kl}) \left| \prod_{i \neq a} \lambda_i \right|. \quad (\text{A13})$$

i.e the flux of critical lines (or the length per unit volume) is given by the average absolute value of the Gaussian curvature of the field in the space orthogonal to the skeleton.

Let us write the probability of measuring the set $\{\lambda_i\}$ as

$$\prod_{i \leq N} d\lambda_i \prod_{i < j} (\lambda_i - \lambda_j) \exp\left(-\frac{1}{2} Q_\gamma(\eta, \{\lambda_i\})\right), \quad (\text{A14})$$

where Q_γ is a quadratic form in λ_i and η which functional form is

$$Q_\gamma(\eta, \{\lambda_i\}) = \eta^2 + \frac{(\sum_i \lambda_i + \gamma\eta)^2}{(1 - \gamma^2)} + \mathcal{Q}_N(\{\lambda_i\}), \quad (\text{A15})$$

and $\prod_{i < j} (\lambda_i - \lambda_j)$ is the Jacobian of the transformation to the Hessian eigenframe. Here \mathcal{Q}_N involves polynomial combinations of the eigenvalues of the traceless part of the Hessian (see Appendix D):

$$\mathcal{Q}_N(\{x_{ij}\}) = \frac{N(N+2)}{2} \sum_{ij} \bar{x}_{ij} \bar{x}_{ij}, \quad \text{with } \bar{x}_{ij} = x_{ij} - \delta_{ij} \frac{1}{N} \sum_i x_{ii}, \quad (\text{A16})$$

which can be rearranged explicitly in terms of λ s as:

$$\mathcal{Q}_N(\{\lambda_i\}) = (N+2) \left[\frac{1}{2} (N-1) \sum_i \lambda_i^2 - \sum_{i \neq j} \lambda_i \lambda_j \right]. \quad (\text{A17})$$

It now follows that the differential length of the ND-critical lines is for the stiff approximation:

$$\frac{\partial \mathcal{L}^{\text{ND}}}{\partial \eta} \propto \left(\frac{1}{R_*}\right)^{N-1} \frac{1}{\sqrt{1-\gamma^2}} \int \cdots \int \prod_{i \leq n} d\lambda_i \prod_{i < j} (\lambda_i - \lambda_j) \left| \prod_{i > 1} \lambda_i \right| \exp\left(-\frac{1}{2} Q_\gamma(\eta, \{\lambda_i\})\right). \quad (\text{A18})$$

Equation (A18) is the formal generalization of equations (30) and (49). For the ND-skeleton, equation (A18) also holds but the integration region should be restricted to the corresponding condition on the sign of the eigenvalues. Since the argument of Q_γ is extremal as a function of η when $\gamma\eta \sim \sum_i \lambda_i$, the largest contribution at large $\gamma\eta$ in the integral should arise when $\lambda_i \propto \gamma\eta$ since near the maximum at high contrast all eigen values are equal (Pichon & Bernardeau 1999). Hence given that $\prod_{i < j} (\lambda_i - \lambda_j)$ is the measure, the only remaining contribution in the integrand comes from $|\prod_{i > 1} \lambda_i| \propto (\lambda\eta)^{N-1}$, and the dominant term at large η is given by

$$\frac{\partial \mathcal{L}^{\text{ND}}}{\partial \eta} \underset{\gamma\eta \rightarrow \infty}{\sim} \frac{1}{\sqrt{2\pi}} \exp\left[-\frac{1}{2}\eta^2\right] \left(\frac{\eta}{R_0}\right)^{N-1},$$

where $R_0 = R_*/\gamma$ is defined in equation (3).

APPENDIX B: SECONDARY CRITICAL LINES IN 2D

In this Appendix we present a study of asymptotic behaviour of the lengths statistics of secondary critical lines for 2D Gaussian field. Secondary critical lines are the ones that have a gradient of the field aligned with the Hessian eigenvector that corresponds to the largest by magnitude eigenvalue, i.e with the direction of maximum curvature of the field. In 2D, this is the direction of λ_2 in the skeleton region, $|\lambda_1| < |\lambda_2|$, and is the direction of λ_1 in the anti-skeleton region. We shall explicitly consider the first type, realizing that the second type is a mirror case with $\eta \rightarrow -\eta$.

Our starting point is the part of expression (27) that corresponds to the lines where the gradient is aligned with the second eigen-direction, in the region when they are secondary, $\tilde{u} > 0$

$$\frac{\partial \mathcal{L}^{\text{sec}}}{\partial \eta} = \frac{4\sqrt{2}}{(2\pi)^{3/2}\sqrt{1-\gamma^2}} \exp[-\eta^2/2] \int_0^\infty d\tilde{w}\tilde{w} \int_0^\infty d\tilde{u} |2\tilde{w} - \tilde{u}| \exp\left[-\frac{(\tilde{u} - \gamma\eta)^2}{2(1-\gamma^2)} - 4\tilde{w}^2\right] . \quad (\text{B1})$$

The absolute value of the transverse to the gradient curvature $2\lambda_1 = 2\tilde{w} - \tilde{u}$ is evaluated differently for $\tilde{u} \leq 2\tilde{w}$ and $\tilde{u} > 2\tilde{w}$. It is convenient to make the inner integration to be over \tilde{w} , since it can be carried out analytically. The integral splits into two terms

$$\frac{\partial \mathcal{L}^{\text{sec}}}{\partial \eta} = \frac{4\sqrt{2}}{(2\pi)^{3/2}\sqrt{1-\gamma^2}} \exp[-\eta^2/2] (I_1 + I_2) , \quad (\text{B2})$$

where

$$I_1 = \int_0^\infty d\tilde{u} \exp\left[-\frac{(\tilde{u} - \gamma\eta)^2}{2(1-\gamma^2)}\right] \int_{\tilde{u}/2}^\infty \tilde{w}(2\tilde{w} - \tilde{u}) d\tilde{w} e^{-4\tilde{w}^2} = \frac{\sqrt{\pi}}{16} \int_0^\infty d\tilde{u} \exp\left[-\frac{(\tilde{u} - \gamma\eta)^2}{2(1-\gamma^2)}\right] \text{Erfc}(\tilde{u}) , \quad (\text{B3})$$

$$I_2 = \int_0^\infty d\tilde{u} \exp\left[-\frac{(\tilde{u} - \gamma\eta)^2}{2(1-\gamma^2)}\right] \int_0^{\tilde{u}/2} \tilde{w}(\tilde{u} - 2\tilde{w}) d\tilde{w} e^{-4\tilde{w}^2} = \frac{\sqrt{\pi}}{16} \int_0^\infty d\tilde{u} \exp\left[-\frac{(\tilde{u} - \gamma\eta)^2}{2(1-\gamma^2)}\right] \left[\frac{2}{\sqrt{\pi}}\tilde{u} - \text{Erf}(\tilde{u})\right] . \quad (\text{B4})$$

so that finally

$$\frac{\partial \mathcal{L}^{\text{sec}}}{\partial \eta} = \frac{1}{4\pi^{3/2}\sqrt{1-\gamma^2}} \exp[-\eta^2/2] \int_0^\infty d\tilde{u} \exp\left[-\frac{(\tilde{u} - \gamma\eta)^2}{2(1-\gamma^2)}\right] \left[\tilde{u} - \sqrt{\frac{\pi}{4}}\text{Erf}(\tilde{u}) + \sqrt{\frac{\pi}{4}}\text{Erfc}(\tilde{u})\right] . \quad (\text{B5})$$

The integrated length of critical lines L^{sec} is obtained by marginalization over all threshold values η . Performing this integration first

$$L^{\text{sec}} = \frac{1}{2\sqrt{2}\pi} \int_0^\infty d\tilde{u} \exp\left[-\frac{\tilde{u}^2}{2}\right] \left[\tilde{u} - \sqrt{\frac{\pi}{4}}\text{Erf}(\tilde{u}) + \sqrt{\frac{\pi}{4}}\text{Erfc}(\tilde{u})\right] = \frac{\sqrt{2} - \text{ArcCot}(2\sqrt{2})}{4\pi} = 0.08550 \quad (\text{B6})$$

Thus secondary critical lines are on average almost three times rarer than the primary ones.

B1 Special cases: $\eta \rightarrow \infty$

At high density thresholds the leading asymptotic behaviour for $\gamma\eta \gg 1$ is obtained by using $\frac{1}{\sqrt{2\pi(1-\gamma^2)}} \exp\left[-\frac{(\tilde{u} - \gamma\eta)^2}{2(1-\gamma^2)}\right] \xrightarrow{\eta \rightarrow \infty} \delta_D(\tilde{u} - \gamma\eta)$. Therefore

$$\frac{\partial \mathcal{L}^{\text{sec}}}{\partial \eta} \xrightarrow{\eta \rightarrow \infty} \frac{1}{\sqrt{2\pi}} \exp[-\eta^2/2] \frac{1}{4} \left(\frac{2}{\sqrt{\pi}}\gamma\eta - 1\right) . \quad (\text{B7})$$

B2 Special cases: $\eta \rightarrow 0$

At small threshold η series representation

$$\exp\left[-\frac{(\tilde{u} - \gamma\eta)^2}{2(1-\gamma^2)}\right] = \exp\left[-\frac{\tilde{u}^2}{2(1-\gamma^2)}\right] \sum_{n=0}^{\infty} \frac{1}{n!(1-\gamma^2)^{n/2}} H_n\left(\frac{\tilde{u}}{\sqrt{1-\gamma^2}}\right) (\gamma\eta)^n , \quad (\text{B8})$$

where Hermite polynomials H_{2n} are taken in probabilistic notation, gives

$$\frac{\partial \mathcal{L}^{\text{sec}}}{\partial \eta}(\eta \rightarrow 0) = \frac{1}{\sqrt{2\pi}} \exp[-\eta^2/2] \sum_{n=0}^{\infty} A_n (\gamma\eta)^n \quad \text{where} \\ A_n \equiv \frac{1}{2\sqrt{2}\pi n!(1-\gamma^2)^{n/2}} \int_0^\infty d\tilde{u} \exp[-\tilde{u}^2/2] H_n(\tilde{u}) \left(\sqrt{1-\gamma^2}\tilde{u} - \sqrt{\frac{\pi}{4}}\text{Erf}\left[\sqrt{1-\gamma^2}\tilde{u}\right] + \sqrt{\frac{\pi}{4}}\text{Erfc}\left[\sqrt{1-\gamma^2}\tilde{u}\right]\right) \quad (\text{B9})$$

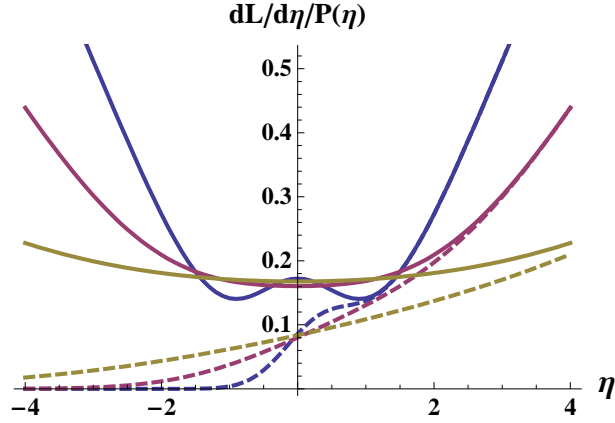


Figure B1. Differential length of the secondary critical lines $\partial\mathcal{L}/\partial\eta/\text{PDF}$ in 2D for the complete set (solid) and the ones with $\nabla\rho$ aligned with λ_2 direction in the skeleton $|\lambda_1| \leq |\lambda_2|$ region (dashed). Different curves from purple to green correspond to the spectral parameter values $\gamma = 0.3, 0.6, 0.95$.

The first three coefficients are

$$\begin{aligned}
 A_0 &= \frac{\sqrt{2(1-\gamma^2)} + \text{acot}[\sqrt{2(1-\gamma^2)}] - \text{atan}[\sqrt{2(1-\gamma^2)}]}{4\pi}, \\
 A_1 &= \frac{1}{4\sqrt{\pi}} \left(1 + \frac{1}{\sqrt{2(1-\gamma^2)}} - \frac{2}{\sqrt{3-2\gamma^2}} \right), \\
 A_2 &= \frac{\sqrt{2}}{8\pi} \frac{1-2\gamma^2}{3-2\gamma^2} (1-\gamma^2)^{-\frac{1}{2}}, \tag{B10}
 \end{aligned}$$

If we add all secondary critical lines, the odd power terms of the expansion (B8) cancel, while the even double recovering symmetrical behaviour of the differential length with the threshold. In Figure B1 this behaviour is illustrated.

Under our definition of the secondary critical lines, for $\gamma > 1/\sqrt{2}$ there is an excess of critical lines near zero threshold. The curvature at $\eta = 0$ is positive and diverges in the limit $\gamma \rightarrow 1$ when our series expansion formally fails. This divergence in the second derivative of the differential length is exactly opposite the one the primary lines demonstrate in this limit. We should emphasize, that near $\eta = 0$ the behaviour of critical lines of individual type depend significantly on how exactly they are defined.

APPENDIX C: ASYMPTOTIC BEHAVIOUR OF CRITICAL LINES IN 3D

There are four regions with the different signs of sorted eigenvalues in 3D: I — ($0 > \lambda_1 \geq \lambda_2 \geq \lambda_3$), II — ($\lambda_1 \geq 0, 0 > \lambda_2 \geq \lambda_3$), III — ($\lambda_1 \geq \lambda_2 \geq 0, 0 > \lambda_3$) and IV — ($\lambda_1 \geq \lambda_2 \geq \lambda_3 \geq 0$). Since \tilde{w} is non-negative, the correspondent zones of integration for equations (48) and (49) are easy to visualize in (\tilde{v}, \tilde{u}) plane (see Figure C1). The integration limits and the integrand acquire the following form

$$\left. \begin{aligned}
 I : & \int_0^\infty d\tilde{w} \int_{-\tilde{w}}^{\tilde{w}} d\tilde{v} \int_0^\infty d\tilde{u} \left[\frac{1}{3}\tilde{u}^2 - \frac{1}{3}\tilde{v}^2 - \tilde{w}^2 \right] \\
 II : & \int_0^\infty d\tilde{w} \int_{-\tilde{w}}^{\tilde{w}} d\tilde{v} \int_{-\tilde{v}+3\tilde{w}}^{\tilde{v}+3\tilde{w}} d\tilde{u} \left[\tilde{w}^2 - \frac{1}{9}(\tilde{u} + \tilde{v})^2 + \frac{2}{3}\tilde{w}(\tilde{u} - 2\tilde{v}) \right] \\
 III : & \int_0^\infty d\tilde{w} \int_{-\tilde{w}}^{\tilde{w}} d\tilde{v} \int_{2\tilde{v}}^{\tilde{v}} d\tilde{u} \left[\tilde{w}^2 - \frac{1}{9}(\tilde{u} + \tilde{v})^2 - \frac{2}{3}\tilde{w}(\tilde{u} - 2\tilde{v}) \right] \\
 IV : & \int_0^\infty d\tilde{w} \int_{-\tilde{w}}^{\tilde{w}} d\tilde{v} \int_{-\tilde{v}-3\tilde{w}}^{-\tilde{v}-3\tilde{w}} d\tilde{u} \left[\frac{1}{3}\tilde{u}^2 - \frac{1}{3}\tilde{v}^2 - \tilde{w}^2 \right]
 \end{aligned} \right\} \times \tilde{w} (\tilde{w}^2 - \tilde{v}^2) \exp \left[-\frac{(\tilde{u} - \gamma\eta)^2}{2(1-\gamma^2)} - \frac{15}{2}\tilde{w}^2 - \frac{5}{2}\tilde{v}^2 \right]. \tag{C1}$$

Changing variables $\tilde{u} \rightarrow -\tilde{u}, \tilde{v} \rightarrow -\tilde{v}$ in III and IV one can combine the last two cases with the first two

$$\left. \begin{aligned}
 I + IV : & \int_0^\infty d\tilde{w} \int_{-\tilde{w}}^{\tilde{w}} d\tilde{v} \int_{3\tilde{w}-\tilde{v}}^{\tilde{v}} d\tilde{u} \left[\frac{1}{3}\tilde{u}^2 - \frac{1}{3}\tilde{v}^2 - \tilde{w}^2 \right] \\
 II + III : & \int_0^\infty d\tilde{w} \int_{-\tilde{w}}^{\tilde{w}} d\tilde{v} \int_{2\tilde{v}}^{3\tilde{w}-\tilde{v}} d\tilde{u} \left[\tilde{w}^2 - \frac{1}{9}(\tilde{u} + \tilde{v})^2 + \frac{2}{3}\tilde{w}(\tilde{u} - 2\tilde{v}) \right]
 \end{aligned} \right\} \times \tilde{w} (\tilde{w}^2 - \tilde{v}^2) \exp \left[-\frac{15}{2}\tilde{w}^2 - \frac{5}{2}\tilde{v}^2 \right] \Phi_\gamma(\tilde{u}, \eta). \tag{C2}$$

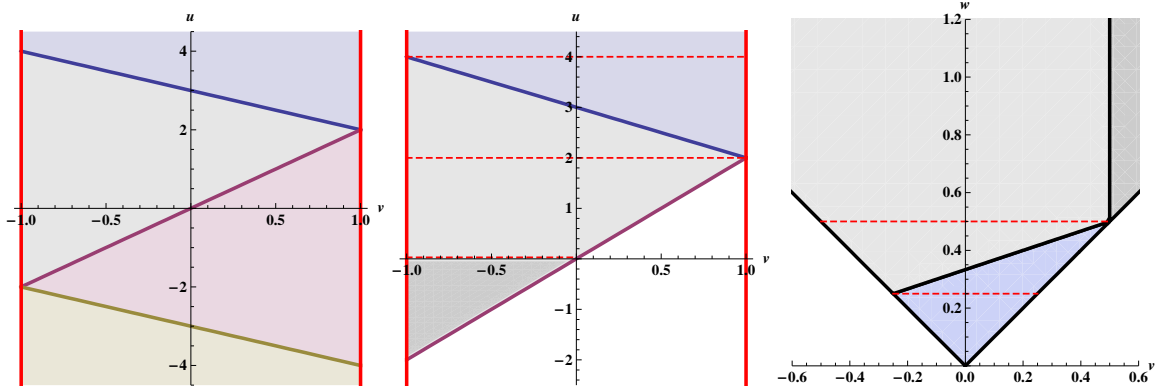


Figure C1. *Left:* Integration zones in \tilde{v}, \tilde{u} plane based on the signs of the eigenvalues. Variables are given in units of \tilde{w} . Here \tilde{v} varies from $-\tilde{w}$ to $+\tilde{w}$, while \tilde{u} is unrestricted. Three inclined lines are (from top to bottom) a) $\lambda_1 = 0 \Rightarrow \tilde{u} = -\tilde{v} + 3\tilde{w}$, b) $\lambda_2 = 0 \Rightarrow \tilde{u} = 2\tilde{v}$ and c) $\lambda_3 = 0 \Rightarrow \tilde{u} = -\tilde{v} - 3\tilde{w}$. In the upper sector I (that stretches to infinity in \tilde{u}) ($0 > \lambda_1 \geq \lambda_2 \geq \lambda_3$), next is the zone II ($\lambda_1 \geq 0, 0 > \lambda_2 \geq \lambda_3$), then III ($\lambda_1 \geq \lambda_2 \geq 0, 0 > \lambda_3$), and, finally extending to minus infinity in \tilde{u} is the sector IV where ($\lambda_1 \geq \lambda_2 \geq \lambda_3 \geq 0$). *Centre:* two zones of integration after variable change leading to equation (C2). Horizontal dashed lines mark the further subdivision of the integration space if the order of integration is changed according to equation (C5). *Right:* Integration zones in the (\tilde{v}, \tilde{w}) plane after \tilde{u} has been mapped to the $[0 - \infty]$ interval. Variables are given in units of \tilde{u} . The lower triangular zone corresponds to semi-open upper band in $\tilde{v} - \tilde{u}$ of the centre panel. In this region, the integrand is given by the terms I+III of equation (C2). Vice-versa, the open upper band in the (\tilde{v}, \tilde{w}) plane corresponds to the II+IV integration over the lower triangular zone in the $\tilde{v} - \tilde{u}$ space. The right-most sector of this region, however, corresponds to negative \tilde{u} , so the integrand in this sector has coordinate change $\tilde{u} \rightarrow -\tilde{u}, \tilde{v} \rightarrow -\tilde{v}$. The dashed lines show the subdivided integrals given in equation (C5), which corresponds to subdivisions in the centre panel.

where

$$\Phi_\gamma(\tilde{u}, \eta) = \exp \left[-\frac{(\tilde{u} - \gamma\eta)^2}{2(1 - \gamma^2)} \right] + \exp \left[-\frac{(\tilde{u} + \gamma\eta)^2}{2(1 - \gamma^2)} \right].$$

Direct evaluation of the integrated length gives

$$L = 0.289627 (\times R_*^{-2}) . \quad (\text{C3})$$

To study high threshold regime it is advantageous to make the \tilde{u} integration the outmost one, since it depends on the variable threshold

$$\begin{aligned} I + IV : & \int_0^\infty d\tilde{w} \int_{-\tilde{w}}^{\tilde{w}} d\tilde{v} \int_{3\tilde{w}-\tilde{v}}^\infty d\tilde{u} \rightarrow \int_0^\infty d\tilde{u} \int_0^{\tilde{u}/4} d\tilde{w} \int_{-\tilde{w}}^{\tilde{w}} d\tilde{v} + \int_0^\infty d\tilde{u} \int_{\tilde{u}/4}^{\tilde{u}/2} d\tilde{w} \int_{3\tilde{w}-\tilde{u}}^{\tilde{w}} d\tilde{v} \\ II + III : & \int_0^\infty d\tilde{w} \int_{-\tilde{w}}^{\tilde{w}} d\tilde{v} \int_{2\tilde{v}}^{3\tilde{w}-\tilde{v}} d\tilde{u} \rightarrow \int_0^\infty d\tilde{u} \int_{\tilde{u}/4}^{\tilde{u}/2} d\tilde{w} \int_{-\tilde{w}}^{3\tilde{w}-\tilde{u}} d\tilde{v} + \int_0^\infty d\tilde{u} \int_{\tilde{u}/2}^\infty d\tilde{w} \int_{-\tilde{w}}^{\tilde{u}/2} d\tilde{v} + \int_0^\infty d\tilde{u} \int_{\tilde{u}/2}^\infty d\tilde{w} \int_{\tilde{u}/2}^{\tilde{w}} d\tilde{v}(\tilde{u}, \tilde{v} \rightarrow -\tilde{u}, -\tilde{v}) . \end{aligned} \quad (\text{C4})$$

The parenthesis in the last term indicate the substitution that must be performed in the integrand. Right panel in Figure C1 illustrates the integration zones now in the (\tilde{v}, \tilde{w}) plane.

Although one can perform the \tilde{v} integral analytically and reduce the problem to two-dimensional integration, the resulting expression is too cumbersome. We can obtain useful limits already from unreduced formulae. In particular, at high density threshold, $\gamma\eta \rightarrow \infty$, only the first integral in the term (C4), which contains $\tilde{w}, \tilde{v} \sim 0$ neighbourhood, is not exponentially small. Moreover, in the leading order the upper limit of the integral over \tilde{w} can be set to infinity.

$$\begin{aligned} \frac{\partial \mathcal{L}}{\partial \eta} & \underset{\gamma\eta \rightarrow \infty}{\sim} \frac{3^2 5^{5/2}}{4\pi^2 \sqrt{2\pi}(1 - \gamma^2)} \exp \left[-\frac{1}{2}\eta^2 \right] \int_0^\infty d\tilde{u} \int_0^\infty d\tilde{w} \int_{-\tilde{w}}^{\tilde{w}} d\tilde{v} \tilde{w}(\tilde{w}^2 - \tilde{v}^2) [\tilde{u}^2 - \tilde{v}^2 - 3\tilde{w}^2] \exp \left[-\frac{(\tilde{u} - \gamma\eta)^2}{2(1 - \gamma^2)} - \frac{15}{2}\tilde{w}^2 - \frac{5}{2}\tilde{v}^2 \right] \\ & \underset{\gamma\eta \rightarrow \infty}{\sim} \frac{1}{\sqrt{2\pi}} \exp \left[-\frac{1}{2}\eta^2 \right] \frac{(\gamma\eta)^2 - \gamma^2}{2\pi} . \end{aligned} \quad (\text{C5})$$

APPENDIX D: JOINT DISTRIBUTION OF THE FIELD AND ITS DERIVATIVES FOR A GRF

The joint point distribution functions that are needed for the study of the critical lines in this paper are $P_0(x, x_{kl})$ and $P_1(x_i, x_{ijk})$, taking into account that for Gaussian random field there is no cross-correlation between odd order derivatives and the field itself or even order derivatives. When considering the curvature of the critical lines, fourth order derivatives, and, thus, more general $P_0(x, x_{kl}, x_{klmn})$ have to be considered. Some well known results in 2D and 3D are first summarized in section D1. More general results can be obtained by resorting to a general framework which is sketched in section D2 and applied in section D3 for the various cases of interest.

D1 Lower order joint distributions

Distribution of the Gaussian field and its second derivative in 3D. The full expression for $P_0(x, x_{kl})$ for the Gaussian field is given in Bardeen et al. (1986). Introducing the variables

$$u \equiv -\Delta x = -(x_{11} + x_{22} + x_{33}), \quad w \equiv \frac{1}{2}(x_{11} - x_{33}), \quad v \equiv \frac{1}{2}(2x_{22} - x_{11} - x_{33}), \quad (\text{D1})$$

in place of diagonal elements of the Hessian (x_{11}, x_{22}, x_{33}) one finds that $u, v, w, x_{12}, x_{13}, x_{23}$ are uncorrelated. Importantly, the field, x is only correlated with $u = \Delta x$ and

$$\langle xu \rangle = \gamma, \quad \langle xv \rangle = 0, \quad \langle xw \rangle = 0, \quad \langle xx_{kl} \rangle = 0, \quad k \neq l, \quad (\text{D2})$$

where γ is the same quantity as in equation (5). The full expression of $P_0(x, x_{kl})$ is then

$$P_0(x, x_{kl}) dx d^6 x_{kl} = \frac{5^{1/2} 15^2}{(2\pi)^{7/2} (1 - \gamma^2)^{1/2}} \exp\left(-\frac{1}{2} [Q_0(x, u) + Q_2(v, w, x_{12}, x_{13}, x_{23})]\right) dx du dv dw dx_{12} dx_{13} dx_{23},$$

with the quadratic forms Q_0 and Q_2 given by

$$Q_0 = x^2 + \frac{(u - \gamma x)^2}{(1 - \gamma^2)} \quad Q_2 = 5v^2 + 15(w^2 + x_{12}^2 + x_{13}^2 + x_{23}^2). \quad (\text{D3})$$

It depends only on a single correlation parameter: γ .

First and third derivatives of the Gaussian field in 3D. A similar procedure can be performed for the joint probability of the first and third derivatives of the fields, $P_1(x_i, x_{ijk})$ by defining the following nine parameters (see also (Hanami 2001)):

$$u_i \equiv \nabla_i u, \quad v_i \equiv \frac{1}{2} \epsilon^{ijk} \nabla_i (\nabla_j \nabla_j - \nabla_k \nabla_k) x, \quad \text{with } j < k, \quad \text{and } w_i \equiv \sqrt{\frac{5}{12}} \nabla_i \left(\nabla_i \nabla_i - \frac{3}{5} \Delta \right) x, \quad (\text{D4})$$

and replacing the variables $(x_{i11}, x_{i22}, x_{i33})$ with (u_i, v_i, w_j) . In that case, the only cross-correlations in the vector $(x_1, x_2, x_3, u_1, v_1, w_1, u_2, v_2, w_2, u_3, v_3, w_3, x_{123})$ which do not vanish are between the same components of the gradient and the gradient of the Laplacian of the field:

$$\langle x_i u_i \rangle = \tilde{\gamma}/3, \quad i = 1, 2, 3, \quad (\text{D5})$$

where $\tilde{\gamma}$ is the same quantity as in equation (5). This allows us to write:

$$P_1(x_i, x_{ijk}) d^3 x_i d^{10} x_{ijk} = \frac{105^{7/2} 3^3}{(2\pi)^{13/2} (1 - \tilde{\gamma}^2)^{3/2}} \exp\left(-\frac{1}{2} (Q_1 + Q_3)\right) d^3 x_i d^3 u_i d^3 w_i d^3 v_i dx_{123}. \quad (\text{D6})$$

with the quadratic forms:

$$Q_1 = 3 \sum_i \left(\frac{(u_i - \tilde{\gamma} x_i)^2}{(1 - \tilde{\gamma}^2)} + x_i^2 \right), \quad Q_3 = 105 \left(x_{123}^2 + \sum_{i=1}^3 (v_i^2 + w_i^2) \right). \quad (\text{D7})$$

The Gaussian field and its second derivative in 2D. Introducing the variables

$$u \equiv -\Delta x = -(x_{11} + x_{22}), \quad w \equiv \frac{1}{2}(x_{11} - x_{22}), \quad (\text{D8})$$

one finds again that u, w, x_{12} are uncorrelated. The expression for $P_0(x, x_{kl})$ is then

$$P_0(x, x_{kl}) dx d^3 x_{kl} = \frac{8}{(2\pi)^2 (1 - \gamma^2)^{1/2}} \exp\left(-\frac{1}{2} [Q_0(x, u) + Q_2(w, x_{12})]\right) dx du dw dx_{12},$$

where the quadratic forms Q_0 and Q_2 are

$$Q_0 = x^2 + \frac{(u - \gamma x)^2}{(1 - \gamma^2)}, \quad Q_2 = 8(w^2 + x_{12}^2). \quad (\text{D9})$$

First and third derivatives of the Gaussian field in 2D. Defining the following 4 uncorrelated parameters:

$$u_i \equiv \nabla_i u, \quad w_i \equiv \nabla_i \left(\nabla_i \nabla_i - \frac{3}{4} \Delta \right) x, \quad (\text{D10})$$

yields

$$P_1(x_i, x_{ijk}) d^2 x_i d^4 x_{ijk} = \frac{128}{(2\pi)^3 (1 - \tilde{\gamma}^2)} \exp\left(-\frac{1}{2} (Q_1 + Q_3)\right) d^2 x_i d^2 u_i d^2 w_i. \quad (\text{D11})$$

with the quadratic forms:

$$Q_1 = 2 \sum_{i=1}^2 \left(\frac{(u_i - \tilde{\gamma} x_i)^2}{(1 - \tilde{\gamma}^2)} + x_i^2 \right), \quad Q_3 = 32 \sum_{i=1}^2 w_i^2. \quad (\text{D12})$$

It is the purpose of the next section to elucidate the nature of these quadratic forms and to show how similar expressions can be obtained for any combination of derivatives in a space of any dimension.

D2 Theory

To proceed further, a more systematic way of computing the correlations between the field derivatives is needed. This can be provided by the harmonic decomposition of symmetric tensors (such as derivative tensors). The main results are outlined hereafter, the reader being referred to Cardoso (2009) for a detailed exposition.

Harmonic decomposition of symmetric tensors. The harmonic decomposition of symmetric tensors amounts to projection onto the irreducible representations of $\text{SO}(n)$. It is obtained in close form as follows. A symmetric tensor T of rank n is associated with a set $\{T^{(\ell)} \mid 0 \leq \ell \leq n, n - \ell \text{ even}\}$ of ‘‘harmonic components’’ where each $T^{(\ell)}$ is a symmetric trace-free tensor of rank ℓ . Index ℓ can be understood as an *angular frequency*. We refer to it as the ‘‘frequency’’ of the component. The harmonic component at frequency $\ell = n - 2k$ of a rank n tensor is obtained as

$$T^{(n-2k)} = \overline{\text{tr}^k T},$$

where $(\text{tr}^k \cdot)$ means applying k times the trace operator (contraction over any pair of indices) and where \overline{T} denotes the traceless part of tensor T . In indexed notations, the first (ranks 0, . . . , 5) de-traced tensors on R^3 are given by $\bar{t} = t$, $\bar{t}_i = t_i$, $\bar{t}_{ij} = t_{ij} - \frac{1}{3} t_{aa} \delta_{ij}$,

$$\bar{t}_{ijk} = t_{ijk} - \frac{3}{5} t_{aa(j} \delta_{kl)}, \quad \bar{t}_{ijkl} = t_{ijkl} - \frac{6}{7} t_{aa(ij} \delta_{kl)} + \frac{3}{35} t_{aabb} \delta_{(ij} \delta_{kl)}, \quad \bar{t}_{ijklm} = t_{ijklm} - \frac{10}{9} t_{aa(ijk} \delta_{lm)} + \frac{5}{21} t_{aabb(i} \delta_{jk} \delta_{lm)}, \quad (\text{D13})$$

with an implicit summation over repeated indices and symmetrization between parenthesized indices (for instance: $t_{aa(j} \delta_{kl)} = [t_{aa(j} \delta_{kl} + t_{aak} \delta_{lj} + t_{aal} \delta_{jk}]/3$ and so on).

Invariant statistics. Let $\mathcal{T} = \{T_0, T_1, \dots\}$ be a set of symmetric tensors which are jointly isotropically distributed. A consequence of isotropy is frequency decoupling: $T_a^{(\ell)}$ is uncorrelated with $T_b^{(\ell')}$ if $\ell \neq \ell'$. Further, at any frequency ℓ , the scalar product $\langle T_a^{(\ell)} \mid T_b^{(\ell)} \rangle$ is invariant under rotations. It is convenient to arrange these products at frequency ℓ into a $m_\ell \times m_\ell$ Gram matrix \widehat{R}_ℓ where m_ℓ denotes the number of tensors in \mathcal{T} having an harmonic component at frequency ℓ (this occurs whenever $\text{rank}(T) - \ell$ is a non-negative even integer):

$$[\widehat{R}_\ell]_{ab} = \langle T_a^{(\ell)} \mid T_b^{(\ell)} \rangle,$$

where indices a and b run only over the m_ℓ relevant values (the specific ordering does not matter). A further consequence of isotropy is that, in the Gaussian case, these matrices form a set of sufficient statistics: the joint distribution of \mathcal{T} can be expressed as a function of those matrices and nothing else, as seen next.

Spectral matrices. The ‘spectral matrix’ R_ℓ at frequency ℓ is defined as the expected value of \widehat{R}_ℓ , that is, $R_\ell = \text{E}(\widehat{R}_\ell)$. For a set \mathcal{T} of symmetric random tensors with a rotationally invariant joint distribution, one finds

$$\mathcal{T}^\dagger \text{Cov}(\mathcal{T})^{-1} \mathcal{T} = \sum_{\ell} w_\ell \text{tr}(\widehat{R}_\ell R_\ell^{-1}),$$

where w_ℓ is a positive scalar, which is equal to $2\ell + 1$ for tensors in R^3 .

Spectral matrices for a GRF. Now, we consider the case when in $\mathcal{T} = \{T_0, \dots, T_Q\}$, the q -th tensor T_q is the q -th derivative at a given point: $t_{i_1 \dots i_n} = \partial^n \rho / \partial r_{i_1} \dots \partial r_{i_n}$ of a stationary random field ρ with spectrum $P(\nu)$. Then \mathcal{T} is a set of isotropically distributed symmetric tensors and each spectral matrix R_ℓ can be expressed as a function of the spectrum. Indeed, if $\ell - q$ and $\ell - q'$ are non negative even integers, matrix R_ℓ has an entry $[R_\ell]_{qq'}$ related to the derivatives of orders q and q' given by

$$[R_\ell]_{qq'} = (-1)^{\frac{q-q'}{2}} g_\ell \sigma_{\frac{q+q'}{2}}^2,$$

with the spectral moments σ_p^2 defined at eq. (4). The geometric factor g_ℓ is the squared ratio $g_\ell = (\|\overline{\xi^\ell}\|/\|\xi^\ell\|)^2$ by which the norm of the ℓ -th tensor product ξ^ℓ of any vector ξ is decreased upon detracting. It is equal to $g_\ell = \ell!/(2\ell - 1)!!$ in dimension $D = 3$. We do not provide explicit expressions for w_ℓ and g_ℓ in arbitrary dimension since only their ratio w_ℓ/g_ℓ is needed and turns out to have a simpler expression than either w_ℓ or g_ℓ :

$$\frac{w_\ell}{g_\ell} = \frac{(2\ell + D - 2)!!}{\ell! (D - 2)!!}. \quad (\text{D14})$$

Some precomputed values are listed in Table D1.

	$\ell = 0$	$\ell = 1$	$\ell = 2$	$\ell = 3$	$\ell = 4$	$\ell = 5$
D=2	1	2	4	8	16	32
D=3	1	3	15/2	35/2	315/8	693/8
D=4	1	4	12	32	80	192
D=5	1	5	35/2	105/2	1155/8	3003/8

Table D1. Values of $w_\ell/g_\ell = (2\ell + D - 2)!!/(\ell! (D - 2)!!)$ in dimensions $D = 2, 3, 4, 5$ for $0 \leq \ell \leq 5$.

Summary and rescaled forms. We collect all previous results into a normalized form. Using the normalized spectral shape parameters of def. (5) and normalized derivative tensors X_n defined as:

$$X_n = \frac{1}{\sigma_n} \nabla^n \rho, \quad \text{i.e.} \quad x_{i_1 \dots i_n} = \sigma_n^{-1} \frac{\partial^n \rho}{\partial r_{i_1} \dots \partial r_{i_n}},$$

one finds that

$$\mathcal{X}^\dagger \text{Cov}(\mathcal{X})^{-1} \mathcal{X} = \sum_\ell \frac{(2\ell + D - 2)!!}{\ell! (D - 2)!!} \text{tr}(\widehat{\Gamma}_\ell \Gamma_\ell^{-1}), \quad \text{with} \quad [\widehat{\Gamma}_\ell]_{pq} = \langle X_p^{(\ell)} | X_q^{(\ell)} \rangle \quad \text{and} \quad [\Gamma_\ell]_{pq} = (-1)^{\frac{p-q}{2}} \gamma_{p,q}. \quad (\text{D15})$$

Note that the diagonal entries of Γ_ℓ are always equal to 1.

Special cases and smaller statistics. Our approach compresses a set of derivative tensors into a set $\widehat{\Gamma}_\ell$ of symmetric matrices of size $m_\ell \times m_\ell$, yielding $\sum_\ell m_\ell(m_\ell + 1)/2$ invariant scalars. There are two special cases where even smaller invariant sufficient statistics can be found.

First, at angular frequency $\ell = 0$, the detraced tensors are just scalars so that, for $\ell = 0$, one has $[\widehat{\Gamma}_0]_{pq} = \langle X_p^{(0)} | X_q^{(0)} \rangle = X_p^{(0)} X_q^{(0)}$. Therefore $\widehat{\Gamma}_0$ actually is a rank-one matrix: $\widehat{\Gamma}_0 = vv^\dagger$ where the entries of vector v are $v_p = X_p^{(0)}$. Hence, at the null frequency, we can further compress the $m_0(m_0 + 1)/2$ statistics (the non-redundant entries of $\widehat{\Gamma}_0$) into m_0 scalars (the entries of v). Of course, the $\ell = 0$ term in the quadratic form also reads:

$$\text{tr}(\widehat{\Gamma}_0 \Gamma_0^{-1}) = v^\dagger \Gamma_0^{-1} v. \quad (\text{D16})$$

Second, there are several cases of interest where $m_\ell = 2$. This happens for instance at $\ell = 0$ with derivative orders 0 and 2, at $\ell = 1$ when considering derivatives of order 1 and 3, at $\ell = 2$ with derivatives of orders 0,2 and 4, etc. Then, for such an ℓ ,

$$\text{tr}(\widehat{\Gamma}_\ell \Gamma_\ell^{-1}) = \text{tr} \left(\begin{bmatrix} \langle a | a \rangle & \langle a | b \rangle \\ \langle b | a \rangle & \langle b | b \rangle \end{bmatrix} \begin{bmatrix} 1 & -\gamma \\ -\gamma & 1 \end{bmatrix}^{-1} \right)$$

where a and b are rank- ℓ tensors and γ is a scalar. Simple algebra yields

$$\text{tr}(\widehat{\Gamma}_\ell \Gamma_\ell^{-1}) = \|a\|^2 + \frac{\|b + \gamma a\|^2}{1 - \gamma^2}, \quad (\text{D17})$$

that is, a form ubiquitous in this paper. However, an equivalent, more regular form is

$$\text{tr}(\widehat{\Gamma}_\ell \Gamma_\ell^{-1}) = \frac{1}{1 - \gamma^2} (\|a\|^2 + \|b\|^2) + \frac{2\gamma}{1 - \gamma^2} \langle a | b \rangle,$$

which has the benefit of stressing that, at such ℓ , a sufficient statistic is only made of *two* invariant scalars, namely $\|a\|^2 + \|b\|^2$ and $\langle a | b \rangle$. In the limit of weak correlation $\gamma \rightarrow 0$, one has, of course, $\text{tr}(\widehat{\Gamma}_\ell \Gamma_\ell^{-1}) = \|a\|^2 + \|b\|^2$. An even more symmetric form, which stresses the decorrelation between $a + b$ and $a - b$ is

$$\text{tr}(\widehat{\Gamma}_\ell \Gamma_\ell^{-1}) = \frac{\|a + b\|^2}{2(1 - \gamma)} + \frac{\|a - b\|^2}{2(1 + \gamma)}.$$

D3 Some applications

We now work out these expressions in some cases of interest.

Derivative of orders 0+2 in 3D. The case $\mathcal{X} = \{X_0, X_2\}$ is the simplest non-trivial case. The theory sketched at sec. D2 applies straightforwardly. In the notations of section D2], we are concerned with frequencies $\ell = 0$ and $\ell = 2$ for which, in 3D, $w_0/g_0 = 1$, $w_2/g_2 = 15/2$ (see table D1). The quadratic form (D15) then reduces to $\text{tr}(\widehat{\Gamma}_0 \Gamma_0^{-1}) + \frac{15}{2} \text{tr}(\widehat{\Gamma}_2 \Gamma_2^{-1})$. For $\ell = 0$, we have here $m_0 = 2$ and we can use the specific form (D17) to work out $\text{tr}(\widehat{\Gamma}_0 \Gamma_0^{-1})$ with $[a, b] = [X_0^{(0)}, X_2^{(0)}] = [x, x_{aa}]$, that is the (normalized) field and the trace of its Hessian. For $\ell = 2$, we have here $m_2 = 1$: we need only scalars. Following expressions (D15) again, we have $\widehat{\Gamma}_2 = \|X_2^{(2)}\|^2 = \|\bar{X}_2\|^2 = \bar{x}_{ab} \bar{x}_{ab}$ and $\Gamma_2 = (-1)^{(2-2)/2} \gamma_{2,2} = 1$. In summary:

$$Q_0 + Q_2 = \text{tr}(\widehat{\Gamma}_0 \Gamma_0^{-1}) + \frac{15}{2} \text{tr}(\widehat{\Gamma}_2 \Gamma_2^{-1}) = x^2 + \frac{(x_{aa} + \gamma x)^2}{1 - \gamma^2} + \frac{15}{2} \bar{x}_{ab} \bar{x}_{ab}, \quad (\text{D18})$$

This is, of course, identical to equation (D3) using the local definitions there. It also shows that the complicated expression for Q_2 in (D3) is nothing but the squared Euclidean norm of the detraced Hessian (with a $15/2$ prefactor).

Result for orders 1+3 in 3D. We take $\mathcal{X} = \{X_1, X_3\}$, that is, the first and third order derivatives of the field. The rescaled harmonic components are

$$\left[\sigma_1^{-1}X_1^{(1)}\right]_i = x_i, \quad \left[\sigma_3^{-1}X_3^{(1)}\right]_i = x_{iaa}, \quad \left[\sigma_3^{-1}X_3^{(3)}\right]_{ijk} = x_{ijk} - \frac{3}{5}x_{aa(i}\delta_{jk)} = \bar{x}_{ijk}.$$

We need frequencies $\ell = 1$ and $\ell = 3$ for which, in 3D, $w_1/g_1 = 3$, $w_3/g_3 = 35/2$ (see table D1). For frequency $\ell = 1$, we have $m_\ell = 2$; matrix Γ_1 is 2×2 with entries given by equation (D15), that is, diagonal entries equal to 1 (as always) and off-diagonal entries given by $(-1)^{(1-3)/2}\gamma_{1,3} = -\tilde{\gamma}$. Since Γ_1 is 2×2 , we can still use equation (D17) and finally obtain In summary:

$$\frac{w_1}{g_1} \text{tr}(\hat{\Gamma}_1\Gamma_1^{-1}) + \frac{w_3}{g_3} \text{tr}(\hat{\Gamma}_3\Gamma_3^{-1}) = 3 \text{tr}\left\{\left[\begin{array}{cc} 1 & -\tilde{\gamma} \\ -\tilde{\gamma} & 1 \end{array}\right]^{-1} \left[\begin{array}{cc} x_i x_i & x_i x_{iaa} \\ x_i x_{ibb} & x_{icc} x_{idd} \end{array}\right]\right\} + \frac{35}{2} \bar{x}_{ijk} \bar{x}_{ijk} \quad (\text{D19})$$

$$= 3 \left(x_i x_i + \frac{(x_{iaa} - \tilde{\gamma} x_i)(x_{ibb} - \tilde{\gamma} x_i)}{1 - \tilde{\gamma}^2} \right) + \frac{35}{2} \bar{x}_{ijk} \bar{x}_{ijk}. \quad (\text{D20})$$

This is consistent with equation (D6) and reveals the meaning of $x_{123}^2 + \sum_{i=1}^3 (v_i^2 + w_i^2)$ as equal to $\frac{1}{6} \bar{x}_{ijk} \bar{x}_{ijk}$ *i.e.* the squared norm of the detraced third derivative tensor (with a prefactor $1/6$).

The results for other combinations of derivatives can be derived in the same way. A few results are listed below without going into much detail.

Result for orders 0+2+4 in 3D. We consider $\mathcal{X} = \{X_0, X_2, X_4\}$. Hoping to improve clarity, we denote $y_{ij} = [\sigma_4^{-1}X_4^{(2)}]_{ij}$, that is, the de-traced contraction of the 4th-order derivative tensor. Explicitly, in 3D:

$$y_{ij} = x_{ijaa} - \frac{1}{3}x_{aabb}\delta_{ij},$$

With this notation and recalling that \bar{x}_{ijkl} denotes the traceless part of x_{ijkl} (the rescaled 4th-order derivative tensor) computed according to the prescription (D13), the quadratic form is

$$\begin{bmatrix} x \\ x_{aa} \\ x_{aabb} \end{bmatrix}^\dagger \begin{bmatrix} 1 & -\gamma & \tilde{\gamma} \\ -\gamma & 1 & -\tilde{\gamma} \\ \tilde{\gamma} & -\tilde{\gamma} & 1 \end{bmatrix}^{-1} \begin{bmatrix} x \\ x_{aa} \\ x_{aabb} \end{bmatrix} + \frac{15}{2} \text{tr}\left\{\left[\begin{array}{cc} 1 & -\hat{\gamma} \\ -\hat{\gamma} & 1 \end{array}\right]^{-1} \left[\begin{array}{cc} \bar{x}_{ij}\bar{x}_{ij} & \bar{x}_{ij}y_{ij} \\ \bar{x}_{ij}y_{ij} & y_{ij}y_{ij} \end{array}\right]\right\} + \frac{315}{8} \bar{x}_{ijkl}\bar{x}_{ijkl}, \quad (\text{D21})$$

where yet another spectral shape parameter has to be defined:

$$\tilde{\gamma} = \frac{\sigma_2^2}{\sigma_0\sigma_4} = \frac{\hat{R}\hat{R}}{R_0R_*} = \frac{\gamma\tilde{\gamma}^2}{\hat{\gamma}},$$

Needless to say that expression (D18) obtained for $\mathcal{X} = \{X_0, X_2\}$ is recovered by cutting the irrelevant terms from equation (D21).

Result for orders 1+3+5 in 3D. To simplify the notations, we introduce local definitions for the derivative tensors and their contractions:

$$y_a = x_{abb}, \quad z_a = x_{abcc}, \quad t_{abc} = x_{abcd},$$

and, proceeding as above, we obtain the quadratic form:

$$3 \text{tr}\left\{\left[\begin{array}{ccc} 1 & -\gamma_{1,3} & \gamma_{1,5} \\ -\gamma_{1,3} & 1 & -\gamma_{3,5} \\ \gamma_{1,5} & -\gamma_{3,5} & 1 \end{array}\right]^{-1} \left[\begin{array}{ccc} x_a x_a & x_a y_a & x_a z_a \\ y_a x_a & y_a y_a & y_a z_a \\ z_a x_a & z_a y_a & z_a z_a \end{array}\right]\right\} + \frac{35}{2} \text{tr}\left\{\left[\begin{array}{cc} 1 & -\gamma_{3,5} \\ -\gamma_{3,5} & 1 \end{array}\right]^{-1} \left[\begin{array}{cc} \bar{x}_{ijk}\bar{x}_{ijk} & \bar{x}_{ijk}\bar{t}_{ijk} \\ \bar{t}_{ijk}\bar{x}_{ijk} & \bar{t}_{ijk}\bar{t}_{ijk} \end{array}\right]\right\} + \frac{693}{8} \bar{x}_{ijklm}\bar{x}_{ijklm} \quad (\text{D22})$$

The 2D case. The theory applies to isotropic fields in any dimension. We have already provided expressions for the spectral moments (4) and the coefficients w_ℓ/g_ℓ of equation (D14). It remains to find detracing coefficients. In the 2D case, the first (ranks $0, \dots, 5$) de-traced tensors on R^2 are given by $\bar{y} = y$, $\bar{y}_i = y_i$, $\bar{y}_{ij} = y_{ij} - \frac{1}{2}y_{aa}\delta_{ij}$,

$$\bar{y}_{ijk} = y_{ijk} - \frac{3}{4}y_{aa(i}\delta_{jk)}, \quad \bar{y}_{ijkl} = y_{ijkl} - y_{aa(ij}\delta_{kl)} + \frac{1}{8}y_{aabb}\delta_{(ij}\delta_{kl)}, \quad \bar{y}_{ijklm} = y_{ijklm} - \frac{5}{4}y_{aa(ijk}\delta_{lm)} + \frac{5}{16}y_{aabb(i}\delta_{jk}\delta_{lm)}. \quad (\text{D23})$$

For the correlation between the field and its Hessian, we proceed as above in 3D with $w_0/g_0 = 1$ and $w_2/g_2 = 4$ given in table D1. Therefore the quadratic form is

$$Q_0 + Q_2 = \text{tr}(\hat{\Gamma}_0\Gamma_0^{-1}) + 4 \text{tr}(\hat{\Gamma}_2\Gamma_2^{-1}) = x^2 + \frac{(x_{aa} + \gamma x)^2}{1 - \gamma^2} + 4 \bar{x}_{ab}\bar{x}_{ab},$$

in agreement with equation (D9). For the case of first and third order derivatives, we read $w_1/g_1 = 2$ and $w_3/g_3 = 8$ from table D1 so that, similar to equation (D19), one finds

$$\frac{w_1}{g_1} \text{tr}(\widehat{\Gamma}_1 \Gamma_1^{-1}) + \frac{w_3}{g_3} \text{tr}(\widehat{\Gamma}_3 \Gamma_3^{-1}) = 2 \text{tr} \left\{ \begin{bmatrix} 1 & -\tilde{\gamma} \\ -\tilde{\gamma} & 1 \end{bmatrix}^{-1} \begin{bmatrix} x_i x_i & x_i x_{iaa} \\ x_i x_{ibb} & x_{icc} x_{idd} \end{bmatrix} \right\} + 8 \bar{x}_{ijk} \bar{x}_{ijk}, \quad (\text{D24})$$

$$= 2 \left(x_i x_i + \frac{(x_{iaa} - \tilde{\gamma} x_i)(x_{ibb} - \tilde{\gamma} x_i)}{1 - \tilde{\gamma}^2} \right) + 8 \bar{x}_{ijk} \bar{x}_{ijk}, \quad (\text{D25})$$

with $\bar{x}_{ijk} = x_{ijk} - \frac{3}{4} x_{aa(i} \delta_{jk)}$ so that $8\bar{x}_{ijk}\bar{x}_{ijk}$ can be checked to equal Q_3 in equation (D12).

The d -dimensional case. We outline some results in the d -dimensional case. The de-tracing formulae can be extended to the d -dimensional case but, in this paper, we will content ourselves with the correlations between the field and its Hessian: $\mathcal{X} = \{X_0, X_2\}$. Therefore, we need only $\ell = 0$ and $\ell = 2$ so that de-tracing remains trivial: the normalized de-traced Hessian given by $\bar{x}_{ij} = x_{ij} - \frac{1}{d} \delta_{ij} x_{aa}$. Hence for the correlation between the field and its Hessian, we obtain the quadratic form

$$\begin{bmatrix} x \\ x_{aa} \end{bmatrix}^\dagger \begin{bmatrix} 1 & -\gamma \\ -\gamma & 1 \end{bmatrix}^{-1} \begin{bmatrix} x \\ x_{aa} \end{bmatrix} + \frac{d(d+2)}{2} \bar{x}_{ab} \bar{x}_{ab}, \quad (\text{D26})$$

which is a straightforward extension of the 3D case of equation (D18). Just recall that γ is now defined in terms of the spectral moments (5) and that de-tracing the Hessian requires a factor $1/d$ instead of $1/3$.